The Study of Events Observed in Cosmic Rays through the Comparison with the prediction of Monte Carlo Event Generators

DOCTORAL PROJECT

DOCTORAL QUALIFYING EXAM

André Vieira da Silva

andsilva@ifi.unicamp.br

University of Campinas
"*Gleb Wataghin*" Institute of Physics
Department of Cosmic Rays and Chronology

May 16, 2018

Abstract

The general objective of this research plan is to study hadronic interactions produced by particles of cosmic radiation, with energy of up to 10^{17} eV, in the laboratory frame, and compare it with the results obtained by experiments on accelerators and with the prediction of the Monte Carlo event generators (PYTHIA and EPOS LHC). Specifically, we intend to study the elementary processes produced by proton-proton, proton-carbon and proton-lead collisions by generators in the region frontal (or fragmentation region) through energy distributions and multiplicity in pseudo-rapidity (angle) for comparison with data collected by the Brazil-Japan Collaboration (CBJ). This project is a natural continuation of the work carried out in the master's degree in 2016. It should be noted that this type of study with CBJ data and its comparison with accelerator data has not been done so far.

Contents

1 Introduction

- In August 1912, Victor Hess made the historic balloon flight that was set to open a new window on matter in the universe.
  He concludes: "The results of the present observations seem to be most readily explained by the assumption that a radiation of very high penetrating power enters our atmosphere from above ... Since I found a reduction ... neither by night nor at a solar eclipse, one can hardly consider the Sun as the origin." (CERN Courier, Jul 18, 2012)
- 9 September 1932, Carl Anderson discovers the positron.
- 1 September 1933, Bruno Rossi: Cosmic rays are positive charged particles.
- 18 July 1938, Pierre Auger and colleagues demonstrate extensive air showers.
- 22 February 1962, John Linsley detects the first 10^{20} eV cosmic ray.

2 Cosmic Rays Physics

Ultra-High Energy Cosmic Rays

In astroparticle physics, an ultra-high-energy cosmic ray (UHECR) is a cosmic ray particle with a kinetic energy greater than 10^{18} eV, far beyond both its rest mass and energies typical of other cosmic ray particles [1].

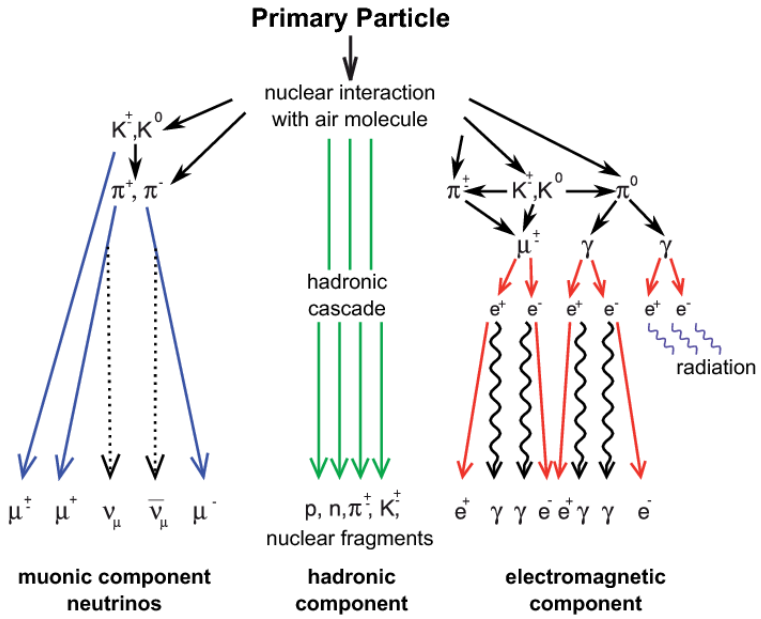

Figure 1: [2]

Chacaltaya Emulsion Chamber Experiment

"Japan-Brazil Collaboration Experiment of Chacaltaya Emulsion Chamber (CBJ) started from a letter of H. Yukawa to C. M. G. Lattes in 1959 proposing a joint experiment of cosmic-rays." (Supplement of the Progress of Theoretical Physics, No. 47, 1971)[3]

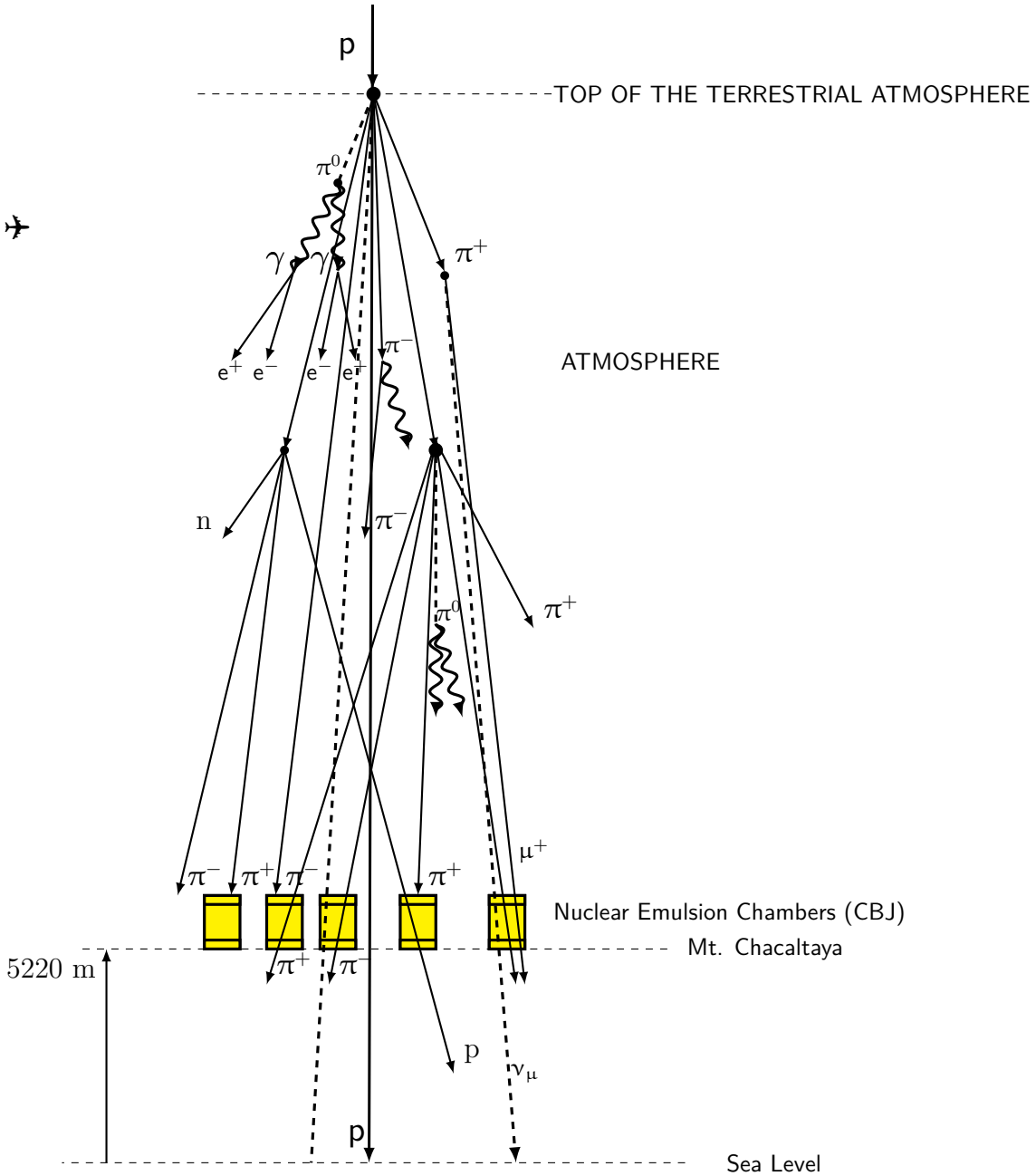

Figure 2: Illustration to describe the interaction of cosmic radiation at the top of the atmosphere, where a cascade of particles produced that propagate in the atmosphere to the level of the detectors (Nuclear Emulsion Chambers) of the CBJ, where the particles are observed.

- Mt. Chacaltaya (5220m, Bolivia).
- CBJ started in 1962 the experiments through the exposures of emulsion chambers to cosmic radiation.
- Emulsion Chamber (Detector: Nuclear Emulsion Plate + X-ray film).
- Phase 1: Emulsion Chamber (Type Simple) A-jets (1962-1970).
- Phase 2: Emulsion Chamber (Chacaltaya two-storey chamber) (Type Producer or a Target) C-jets (1970-88) (CBJ data available) [4].
- Morphological studies of cosmic rays on investigation of atmospheric nuclear interactions through observation of γ-ray families, observed in the detector.
- $E_\gamma \sim E_0/3$, E_0 is the total energy of the cosmic radiation incident in the two-storey chamber.

Chacaltaya Two-Storey Chamber

a. Upper Chamber (7 cm Pb)

b. Carbon Layer (23 cm)

c. Air-gap ($\sim$ 152 cm)

d. Lower Chamber (7 cm Pb) (**LAB Frame**)

82 events with (x, y, E) measurements of electromagnetic showers (Lower Chamber)

$$20 \text{ TeV} \lesssim E_\gamma \lesssim 123 \text{ TeV} \rightarrow 60 \text{ TeV} \lesssim E_0 \lesssim 370 \text{ TeV}$$

- 20 - 30 TeV $\rightarrow$ 36 Events (44 %) $\Rightarrow E_0 \sim 80$ TeV (PYTHIA 8 Simulation/CBJ Data).
- Cosmic rays are highly energetic radiations that can produce particle showers ($\pi^0, \pi^\pm, \mathrm{n}, \mathrm{p}, \gamma, \mathrm{e}^\pm, \eta^0, \mathrm{K}^\pm, ...$) in the earthly atmosphere, through hadronic interactions. Cosmic rays are composed mainly of protons and atomic nuclei at high energies, some particles have an ultra-kinetic kinetic energy, extending up to 10^{20} eV [5].
- To study the hadronic interactions using cosmic radiation as a source of particles, the CBJ[1] used nuclear emulsion chambers to detect the products of the collision of the primary particle, see Figure 3.

[1] Brazil-Japan Cosmic Rays Collaboration (1962-88) [3].

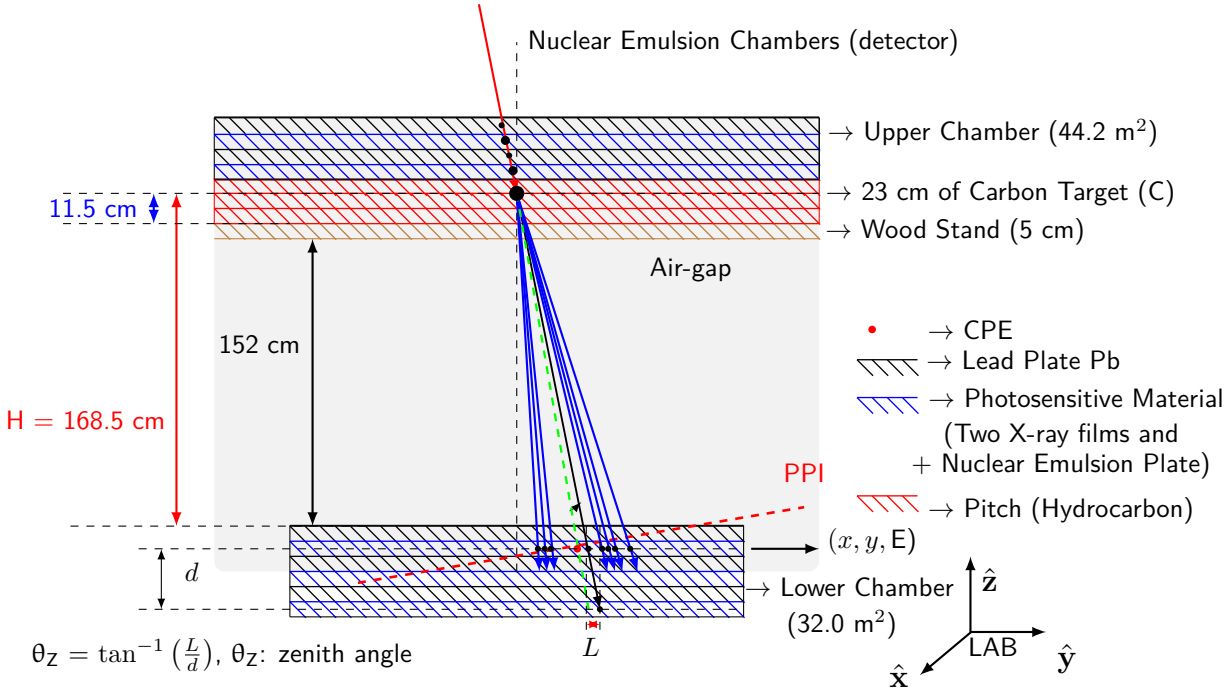

Figure 3: The description of an event type observed in the lower chamber of the emulsion chamber, where the interaction of a primary particle incident in the upper chamber from the extensive atmospheric shower with the material (Lead (Pb) or Carbon (C)) of the detector occurs in the upper chamber, initiating an electromagnetic cascade in the detector. The CBJ adopted that the average position of the vertices interaction coincides with the central region of the carbon target, around 11.5 cm. Figure based on reference [3] and withdrawal of the master's thesis Estudo de Processos Difrativos em Interações Hadrônicas.

2.1 Characteristics of the Events Observed in the CBJ Emulsion Chamber

- Due to the properties of the materials for detection (X-ray Film and Emulsion Plate) there is an energy threshold around 0.5 TeV, i.e., in the event particles with energy below 0.5 TeV are not detected.
- With this experimental characteristic only a part of the energy of the events was observed, in the form of electromagnetic cascades (showers) are in the range of 20 and 123 TeV (see Table 3), approximately, in the LAB frame. In experiments with emulsions, the primary particle interaction energies (incident in the upper chamber) are in the range of approximately 60 to 370 TeV, in the LAB frame.
- Particle flow(or Luminosity) is very low, so the signal-to-noise ratio is very favorable (Low Pileup [2]).
- The interaction of the products of the primary particle in the upper chamber produces secondary ones that are scattered at low angles (or at high pseudo-rapidity values) (frontal region),

[2]The overlap of secondary pp collisions in the primary interaction.

see Figure 3.

- The events observed by the CBJ in the frontal region have particles with low transverse momentum (below 1 GeV approximately) [3]. The low transverse momentum in the events of the CBJ is an evidence to compare with diffractive events in hadronic interactions **softQCD** predicted by the PYTHIA 82 [6] or EPOS LHC [7].

3 Objectives

3.1 General

The general objective of this research plan is to study hadronic interactions produced by particles of cosmic radiation, with energy of up to 10^5 TeV, in the LAB frame, and compare it with the results obtained by the accelerators and Monte Carlo event generators (PYTHIA 82 [6] and EPOS LHC [7]).

3.1.1 Specific

- Through simulations with the event generators we are interested in searching for multiplicity and energy distributions in pseudo-rapidity range that are characteristics of diffractive phenomena, jet production or other asymmetries predicted by the Standard Model or beyond the Standard Model for the energy range approximately of $E_{LAB} \sim 60$ TeV - 370 TeV ($\sqrt{s} \sim 194$ GeV - 694 GeV) in the region forward maybe can help to understand the air shower development of ultra-high energy cosmic rays [8–10]; comparison of cosmic ray to acelerator data [11].
- These samples produced by simulation will be compared with the CBJ experimental data. The bridge between theoretical prediction and observations is done by event generators or via algorithm anti-k_t [12] of the FastJet package [13] for identification of jets or structures, which have few adjustable parameters.
- The aspect of asymmetry in the emission of particles can be used to study the formation of jets, through algorithms of identification of jets, allow to obtain predictions of QCD and the Standard Model related to the configurations of quarks and gluons in hadronic structures, according to can be seen in the article [14].

4 Methodology

This project will have the following phases:

- Collection of information on individual processes of hadronic physics through the event generators. The basic physical process is chosen in the generator, obtaining the multiplicity and energy distributions in pseudo-rapidity. The Monte Carlo event generators are:

  a. **PYTHIA 8.226**[3]
     - It is a program for the generation of high energy physics events, that is, for the description of collisions between particles, such as positron-electron (e^+e^-), proton-proton (pp), proton-antiproton ($p\bar{p}$) and among other combinations (except for heavy-ion collisions (proton-Lead (pPb), proton-Carbon (pC) or Lead-Lead (PbPb)), which is performed by other generators, e.g., EPOS LHC [7]).
     - Contains theories and models for various aspects of physics, such as QCD interactions[4] that includes **SoftQCD** and **HardQCD** processes [15]. A complete list and a description of the processes can be found on the **PYTHIA 8 online manual - Theoretical Physics - Lund University**

  b. **PYTHIA 8.230** (6 October 2017)[5] A new Heavy Ions machinery has been added, that allows PYTHIA to generate pA and AA collisions within a simple model. The new capabilities are pp, pPb, PbPb and pC and among others collisions. Extending the Multiparton Interactions framework with Glauber model [16–18].

  c. **CRMC** ("Cosmic Ray Monte Carlo Package")[6], which is a set of generators that the models of particle production in hadronic collisions most used for studies of showers atmospheres of very high energies. These models are based on the Parton based Gribov-Regge theory [19] and mainly include EPOS-1.99 [20] and EPOS-LHC [7], SIBYLL 2.1 [21] e QGSJET II.04 [22].

- All these models are post-LHC generators tuned by using the LHC Run 1 data ($\sqrt{s} = 7, 8$ TeV).

- Comparison the prediction of the Monte Carlo Event Generators with experimental data from the detectors ATLAS [23], ALICE [24], CMS [25], LHCb [26] and among other through the **RIVET** [27].

  - The **RIVET** toolkit (Robust Independent Validation of Experiment and Theory) is a system for validation of Monte Carlo event generators. It provides a large (and ever growing) set of experimental analyses useful for MC generator development, validation, and tuning, as well as a convenient infrastructure for adding your own analyses. Rivet is the most widespread way by which analysis code from the LHC and other high-energy collider experiments is preserved for comparison to and development of future theory models. It is used by phenomenologists, MC generator developers, and experimentalists on the LHC and other facilities.

[3] The version of PYTHIA used is available on the: http://home.thep.lu.se/~torbjorn/pythia8/pythia8226.tgz

[4] Quantum Chromodynamics: Describes the strong interaction between quarks and gluons.

[5] http://home.thep.lu.se/~torbjorn/Pythia.html.

[6] web.ikp.kit.edu/rulrich/crmc.html

5 Data Treatment Description of an Event CBJ

a. Each event have N shower with position [cm] and energy [TeV] measurements (x_i, y_i, E_i).

b. Weighted Center of Energy (CPE) is $(x_{\mathrm{CPE}}, y_{\mathrm{CPE}})$, in the Laboratory (LAB) frame is:

$$x_{\mathrm{CPE}} = \frac{\sum_i^N x_i \mathrm{E}_i}{\mathrm{E_T}} \ [\mathrm{cm}], \quad y_{\mathrm{CPE}} = \frac{\sum_i^N y_i \mathrm{E}_i}{\mathrm{E_T}} \ [\mathrm{cm}], \tag{1}$$

where $\mathrm{E_{TOTAL}} = \sum_i^N (\mathrm{E}_i)_\gamma$ the total energy of the event in electromagnetic showers (γ). The transformation to CPE frame:

$$x_{ci} = x_i - x_{\mathrm{CPE}}, \quad y_{ci} = y_i - y_{\mathrm{CPE}}. \tag{2}$$

The transformed coordinates (x_{ci}, y_{ci}) for the CPE frame were projected on the PPI, i.e, the event is observed in the frontal plane. By this we calculate the kinematic variables of the event.

c. Azimuth Angle (ϕ_i):

$$\phi_i = \tan^{-1}\left(\frac{y_i'}{x_i'}\right). \tag{3}$$

d. Angle of Scattering (or polar angle) (θ_i):

$$\theta_i = \tan^{-1}\left(\frac{\sqrt{x_i'^2 + y_i'^2}}{\mathrm{h}}\right), \tag{4}$$

being $\mathrm{h} = \mathrm{H}/\cos\theta_{\mathrm{Z}}$ is the height between the half of the Carbon target (C) and the PPI.

e. pseudorapidity (η_i):

$$\eta_i = -\ln\left[\tan\left(\frac{\theta_i}{2}\right)\right]. \tag{5}$$

f. The kinematic variables calculated by the following approximation $\mathrm{E} \approx |\vec{\mathrm{p}}\,|$:

$$\begin{cases} \mathrm{p_{T}}_i = \mathrm{E}_i \sin\theta_i, & (6a) \\ \mathrm{p_x}_i = \mathrm{p_{T}}_i \cos\phi_i, & (6b) \\ \mathrm{p_y}_i = \mathrm{p_{T}}_i \sin\phi_i, & (6c) \\ \mathrm{p_z}_i = \mathrm{E}_i \cos\theta_i. & (6d) \end{cases}$$

All variables previously calculated are in the LAB frame.

6 Kinematic Relativistic Definitions

6.1 Spherical Coordinate System

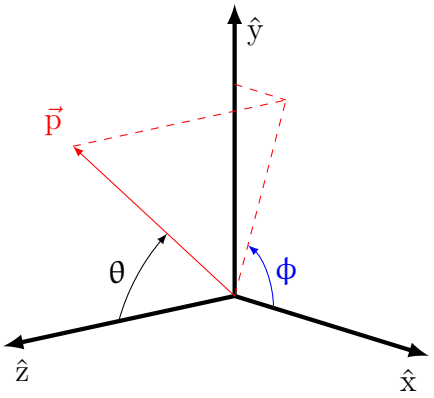

Figure 4: Spherical Coordinate System. $\phi = [-\pi, \pi]$ and $\theta = [0,\ \pi]$

LAB Frame

- Four-momentum: (E, p_x, p_y, p_z), Tranverse momentum: $p_T = \sqrt{p_x^2 + p_y^2}$.
- rapidity: $y \equiv \frac{1}{2} \ln\left[\frac{E+p_z}{E-p_z}\right]$, $\phi = \tan^{-1}\left(\frac{p_y}{p_x}\right)$ $\theta = \tan^{-1}\left(\frac{p_T}{p_z}\right)$.
- Highly Relativistic Particles, $y \simeq \eta = -\ln\left[\tan\left(\frac{\theta}{2}\right)\right]$, LHC or Cosmic Rays.
- LORENTZ INVARIANT $\Delta\eta$: sob the class of Lorentz boosts (Lorentz Transformation).
- In Cosmic Ray: $\theta_\gamma \lesssim 10^{-3}$ rad [28] (High $\eta \gtrsim 7.6$) (Forward) for detectors of the LHC [10].

Lorentz Transformation (LT) LAB $\rightarrow$ CM

$$\vec{\beta}_{CM} = (\beta_x, \beta_y, \beta_z) = \left(\frac{v_x}{c}, \frac{v_y}{c}, \frac{v_z}{c}\right) = \frac{\vec{v}_{CM}}{c} \qquad \gamma_{CM} = \frac{1}{\sqrt{1-\beta_{CM}^2}}$$

or

$$\vec{\beta}_{CM} = \frac{\sum_i^N \vec{p}}{\sum_i^N E_i}, \quad \gamma_{CM} = \frac{\sum_i^N E_i}{\sqrt{s}}, \quad \sqrt{s} = \sqrt{2mE_{LAB}}, \quad E_{LAB} = \sum_i^N E_i$$

$$\sqrt{s} = \sqrt{\left(\sum_i^N E_i\right)^2 - \left(\sum_i^N \vec{p}_i\right)^2}$$

$$\begin{bmatrix} E^* \\ p_x^* \\ p_y^* \\ p_z^* \end{bmatrix} = \begin{bmatrix} \gamma & -\beta_x\gamma & -\beta_y\gamma & -\beta_z\gamma \\ -\beta_x\gamma & 1+(\gamma-1)\frac{\beta_x^2}{\beta^2} & (\gamma-1)\frac{\beta_x\beta_y}{\beta^2} & (\gamma-1)\frac{\beta_x\beta_z}{\beta^2} \\ -\beta_y\gamma & (\gamma-1)\frac{\beta_y\beta_x}{\beta^2} & 1+(\gamma-1)\frac{\beta_y^2}{\beta^2} & (\gamma-1)\frac{\beta_y\beta_z}{\beta^2} \\ -\beta_z\gamma & (\gamma-1)\frac{\beta_z\beta_x}{\beta^2} & (\gamma-1)\frac{\beta_z\beta_y}{\beta^2} & 1+(\gamma-1)\frac{\beta_z^2}{\beta^2} \end{bmatrix} \begin{bmatrix} E \\ p_x \\ p_y \\ p_z \end{bmatrix}$$

$$p_T^* = \sqrt{(p_x^*)^2 + (p_y^*)^2}, \quad \phi^* = \tan^{-1}\left(\frac{p_y^*}{p_x^*}\right) \quad \theta^* = \tan^{-1}\left(\frac{p_T}{p_z^*}\right), \quad \eta_{CM} = -\ln\left[\tan\left(\frac{\theta^*}{2}\right)\right]$$

$$\eta_{CM} = \eta_{LAB} - \frac{1}{2}\ln\left[\frac{1+\beta}{1-\beta}\right]$$

CM Frame

$$p_T = p_T^* \qquad \phi = \phi^* \qquad \sum_{i=1}^{N} \vec{p}_i{}^* = \vec{0} \qquad \sum_{i=1}^{N} E_i^* = \sqrt{s}$$

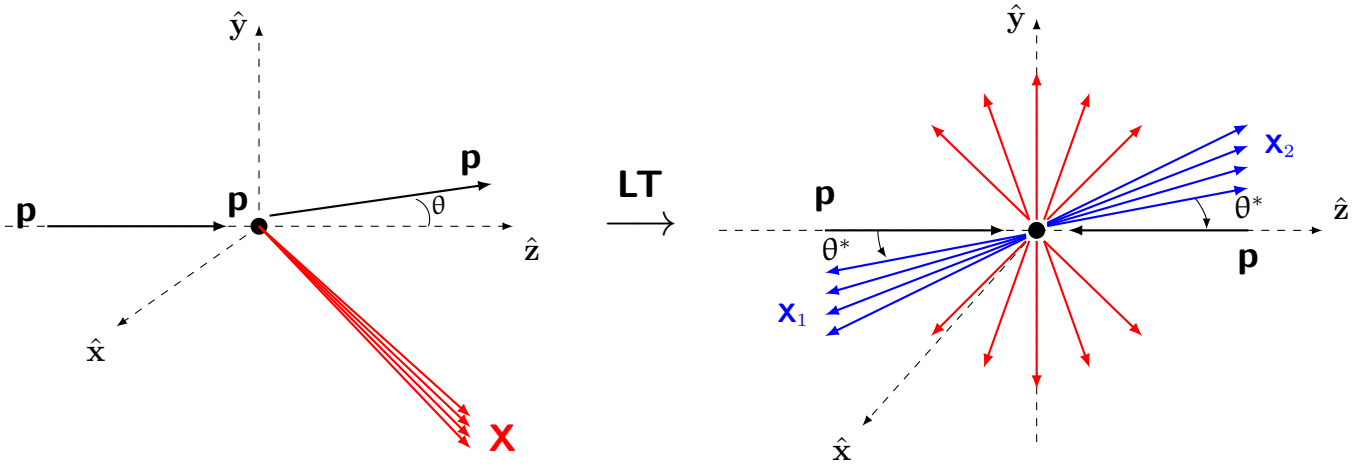

(a) **LAB** (b) **CM**

Figure 5: (a) An incident proton (**p**) collides with a stationary proton proton (**p**) in the LAB frame. (b) Collision of a proton (**p**) with another proton (**p**) in the CM frame. At the point of interaction occurs the multiple production of particles that come out in all directions, a special case is the jet production (the jets are $\mathbf{X}_1$ e $\mathbf{X}_2$).

7 Overview: The Standard Model of Particle Physics

Standard Model

- The Standard Model explains how the basic building blocks of matter interact, governed by three fundamental forces [29, 30].

Table 1: Elementary Particles of the Standard Model

Fermions[a]

Leptons			Quarks		
Particle	**Charge***	**Mass****	**Particle**	**Charge***	**Mass****
electron (e^-)	-1	0.0005	down (d)	-1/3	0.003
electron neutrino (ν_e)	0	$< 10^{-9}$	up (u)	+2/3	0.005
muon (μ^-)	-1	0.106	strange (s)	-1/3	0.1
muon neutrino (ν_μ)	0	$< 10^{-9}$	charm (c)	+2/3	1.3
tau (τ^-)	-1	1.78	botton (b)	-1/3	4.5
tau neutrino (ν_τ)	0	$< 10^{-9}$	top (t)	+2/3	174

*In unit of elementary charge e. **Units of GeV. Particle Data Group (PDG) [31].

[a]These particles are characterized by spin $\frac{\hbar}{2}$, described by the Dirac equation, for more details see reference chapter 4 [29].

Table 2: The four interactions of nature with the relative approximate intensities for the interaction between two protons, at a distance of 1 fm = 10^{-15} m (approximately the radius of the proton) and the bosons associated to each interaction.

Interaction	**strength**	**Boson**	**Spin***	**Mass****	**Particle**
Strong	1	gluon (g)	1	0	Quarks
Electromagnetic	10^{-3}	fóton (γ)	1	0	Quarks e Léptons (Carregados)
Weak	10^{-8}	bóson W (W^+, W^-)	1	80.4	Quarks e Léptons
		bóson Z (Z^0)	1	91.2	Quarks e Léptons
Gravitation	10^{-37}	Graviton? (G)	2	0	Quarks e Léptons

*In units of $\hbar$.** units of GeV.

7.1 Quantum Chromodynamics (QCD)

- QCD: Quantum field theory of strong interactions [15, 32, 33].

  - interaction carried by gluons acting on quarks and gluons

- QCD running coupling strength α_s depends on energy [34]
  - Low energy (= long distance or time)
    $\rightarrow$ α_s is large (confinement): non-perturbative regime of QCD (non-pQCD)
  - High energy (= short distance or time)
    $\rightarrow$ α_s is small (asymptotic freedom): perturbative regime of QCD (pQCD)

- pp collisions
  - Two beams of partons (quarks, gluons) initiate the parton-level interaction [35].
  - The bulk of particle production in high-energy hadronic collisions can still not be calculated within first-principles QCD. Phenomenological models based on general principles such as unitarity and analyticity are often combined with perturbative QCD predictions for high-p_T processes to obtain an almost complete description of the final states [35].

- Inelastic hadronic collisions are usually classified into soft processes and hard processes.
  - hard QCD treated within a theoretical framework based on pQCD (high-p_T) [14, 36].
  - However, pQCD is inadequate for describing soft processes such as diffractive dissociation (soft QCD). Instead, the phenomenology of soft hadronic processes based on Gribov-Regge theory [19] has been employed to describe these processes at high energies, e.g, EPOS LHC [7].
  - PYTHIA 82 [6] is intented to describe all components of the total cross section ($\sigma_{\mathrm{Tot}}(s)$) in hadronic collisions, including cross section for elastic scattering ($\sigma_{\mathrm{el}}(s)$) and cross section for diffractive and non-diffractive topologies ($\sigma_{\mathrm{inel}}(s)$) [37]:

$$\sigma_{\mathrm{Tot}}(s) = \sigma_{\mathrm{el}}(s) + \sigma_{\mathrm{inel}}(s), \tag{7}$$

    $\sigma_{\mathrm{Tot}}(s)$ with CM energy squared (s), in units of GeV^2.

$$\sigma_{\mathrm{inel}}(s) = \sigma_{\mathrm{ND}}(s) + \sigma_{\mathrm{SD}}(s) + \sigma_{\mathrm{DD}}(s) + \sigma_{\mathrm{DC}}(s), \tag{8}$$

    with the following cross section for the processes: $\sigma_{\mathrm{ND}}(s)$: Non-Diffractive, $\sigma_{\mathrm{SD}}(s)$: Single-Diffractive, $\sigma_{\mathrm{DD}}(s)$: Double-Diffractive and $\sigma_{\mathrm{DC}}(s)$: Central-Diffractive [38].
  - Diffractive processes are caracterised by rapidity gaps ($\Delta\eta$) in the final state of multiplicity and energy distribuition [**Albrow:2006xt**].

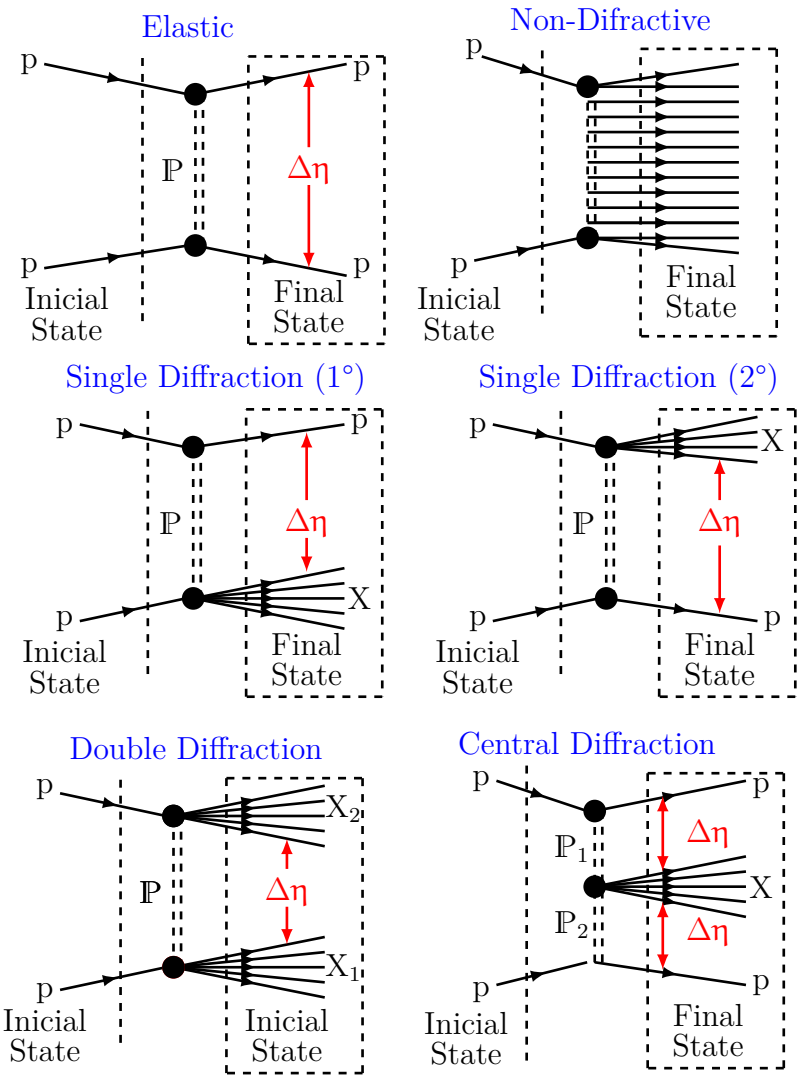

Figure 6: Non-Diffractive and Diffractive processes.

8 Overview: PYTHIA 8

PYTHIA 82

The PYTHIA program is a standard tool for the generation of events in high-energy collisions between elementary particles, comprising a coherent set of physics models for the evolution from a few-body hard-scattering process to a complex multiparticle final state [6].

- Collisions between particles, (e^+e^-), (pp), $(p\bar{p})$ and $\mu^+\mu^-$.
- The particles are produced in vacuum.
- Simulation of the interaction of the particles produced with detector material is not included in PYTHIA.
- Physics come from theory, while other parts are based on phenomenological models, with parameters to be determined from data ("Tuning").

PYTHIA 82

- PYTHIA's physics modeling up $\sqrt{s} = 100$ TeV, corresponding to a pp fixed-target beam energy 10^7 TeV.
- The task of a Monte Carlo event generator is to calculate everything that happens in a high-energy collision, from the hard short-distance physics to the long wavelengths of hadronisation and hadron decays [35, 39].

8.1 Processes

A typical hadronic event generator simulates the following subprocesses:

- Initial-state composition and substructure
- Initial-state radiation
- The hard process
- Resonance decay
- Final-state radiation
- Accompanying semi-hard processes
- Hadronization and further decay

- **HardQCD**: QCD at high energy scales, $Q \gg \Lambda_{QCD} \sim 200$ MeV, is perturbative quantum field theory, the starting point for which is Matrix Elements (MEs) which can be calculated systematically at fixed orders (FO) in the strong coupling α_s. This set of procedures within PYTHIA8 contains the **jet production of QCD** [40] above a minimum threshold of p_T(transverse momentum). The cut $p_{T\,min}$ can not be placed too low, or otherwise reasonably large shock sections will be obtained. This is because the shock section of the perturbative QCD is divergent for p_T in the range of 0.1 - 1 GeV [14, 15], without regularization modifications. The trigger Trigger conditions [41] (experimental cuts) also establish values of p_T Minimum. In the article [42] a study of these sub-processes is carried out through PYTHIA8 to estimate the contribution of each subprocess to the formation of jets.

Jet Definition [13]:

Jets are the collimated sprays of hadrons that result from the fragmentation of a high-energy quark or gluon.

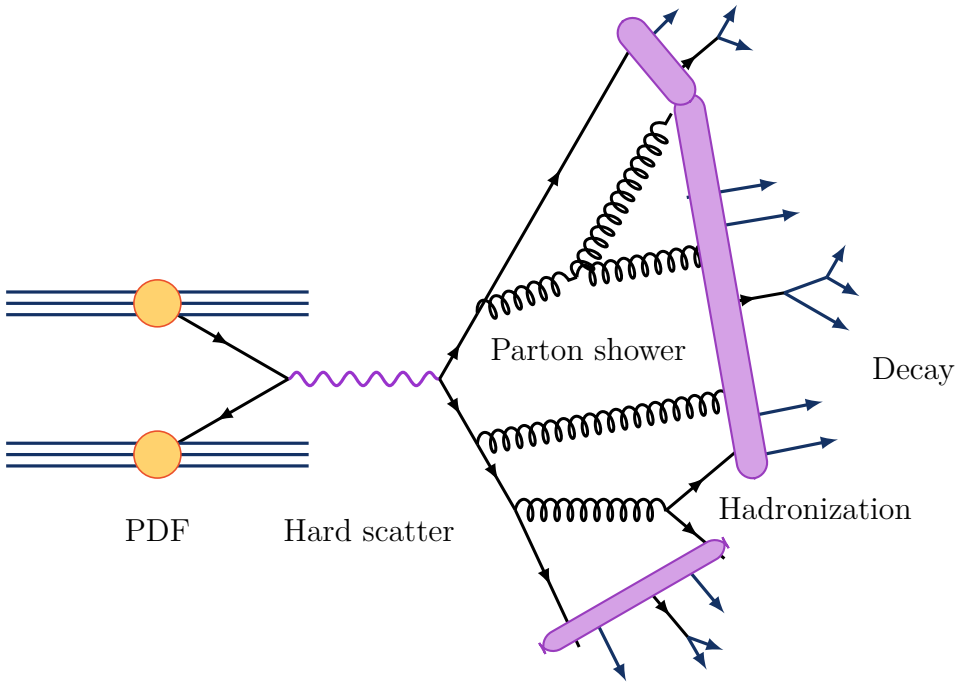

Figure 7: A pictorial representation of a collision with the hard interaction and the resulting fragmentation, hadronization, and decay [Kira Grogg].

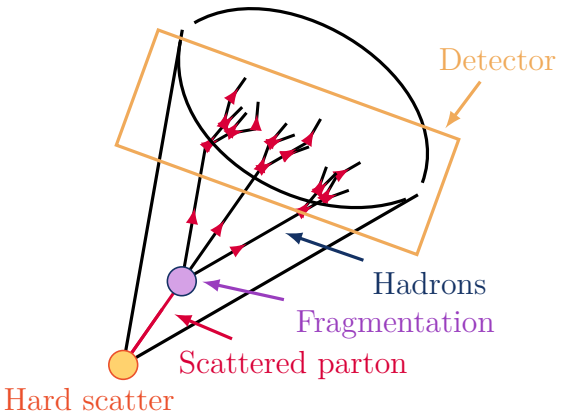

Figure 8: Illustration of the evolution from the hard scattering parton to the jet in the detector [Kira Grogg].

- At lower energies it is difficult to separate the jets from the other 'underlying' hadrons in the event. In order to look for jets one selectes experimentaly events with high-momentum tracks.
- LHC - jet production is the dominant high tranverse-momentum p_T processes [43].
- Jet cross sections serve as one of the main observables in high-energy particle physics, providing precise information on the structure of the proton. Naturally, any measurement of jet energy and momenta leads to a close estimation of the dynamical properties associated with partons [44].

  - Jet clustering algoritms are among the main tools for analysing data from hadronic collisions [45]. In QCD studies, jets are basically the transformed states of partons to hadrons through the hadronization process with produces a collection of spray of particles [44].

- **SoftQCD**: Diffractive and non-diffractive events with low transverse momentum (Minimum Bias). These processes are dominant in the hadron colliders. Most of the events observed in the LHC are due to low-p_T collisions or nonperturbative QCD (only phenomenological models).

  - softQCD = low momentum transfer.
  - These are the dominant types of interaction at hadron colliders.
  - cross-section for any interaction (dominated by soft-QCD).
  - Diffractive scattering in more peripheral pp interactions, where one or both protons survive the interaction and/or are excited into a low-mass state, accounts for 15-40 % [46, 47] of the pp inelastic cross section.
  - An experimental signature for diffraction is given by rapidity gaps [48].
  - As the particle multiplicity produced in these processes is modeled phenomenologically in the existing Monte Carlo (MC) event generators of hadronic interactions, experimental results provide an important input for tuning of the models [49].
  - In the region forward, where diffractive interactions contribute and where most of the interaction energy is going, all the models are fairly close together [50]. This is the motivation to study and analysis the events from cosmic rays observed by the CBJ and compared with predicted hadronic interaction models.
  - Thus the measured hadronic elastic and total cross sections have become crucial instruments to probe the so called soft part of QCD physics, where quarks and gluons are confined, and have led to test and refine Regge behavior and a number of diffractive models [51].

9 PYTHIA 82: Scattering Processes

9.1 SoftQCD

9.1.1 $\mathbf{E_{LAB} = 20\ TeV \rightarrow \sqrt{s} = 193.73\ GeV}$

- 82 pp collisions in the LAB reference (82 C-jets events), $E_{cut} = 0.5$ TeV.
- Beam 1 ($E_{BEAM\ 1} = 20$ TeV), Beam 2 ($E_{BEAM\ 2} = m_p = 0.9383$ GeV), $\gamma_{CM} = 103.24$, $\beta_{CM} = 0.9999533089$.
- $\sqrt{s} = \sqrt{2m_pE} = \sqrt{2 \cdot 0.9383 \cdot 20.10^3} = 193.73$ GeV.

```
*-------  PYTHIA Event and Cross Section Statistics  ---------------*
| Subprocess                          events   |      sigma +- delta       |
|                                              |     (estimated) (mb)       |
|------------------------------------------------------------------------|
| non-diffractive                       49     |   2.852e+01  1.274e-07     |
| p p -> p p elastic                    14     |   9.359e+00  5.518e-08     |
| p p -> X p single diffractive          6     |   4.627e+00  0.000e+00     |
| p p -> p X single diffractive          4     |   4.627e+00  0.000e+00     |
| p p -> X X double diffractive          9     |   4.167e+00  0.000e+00     |
|------------------------------------------------------------------------|
# sum                                  82     |   5.130e+01  1.389e-07     |
*--------  End PYTHIA Event and Cross Section Statistics -----------*
```

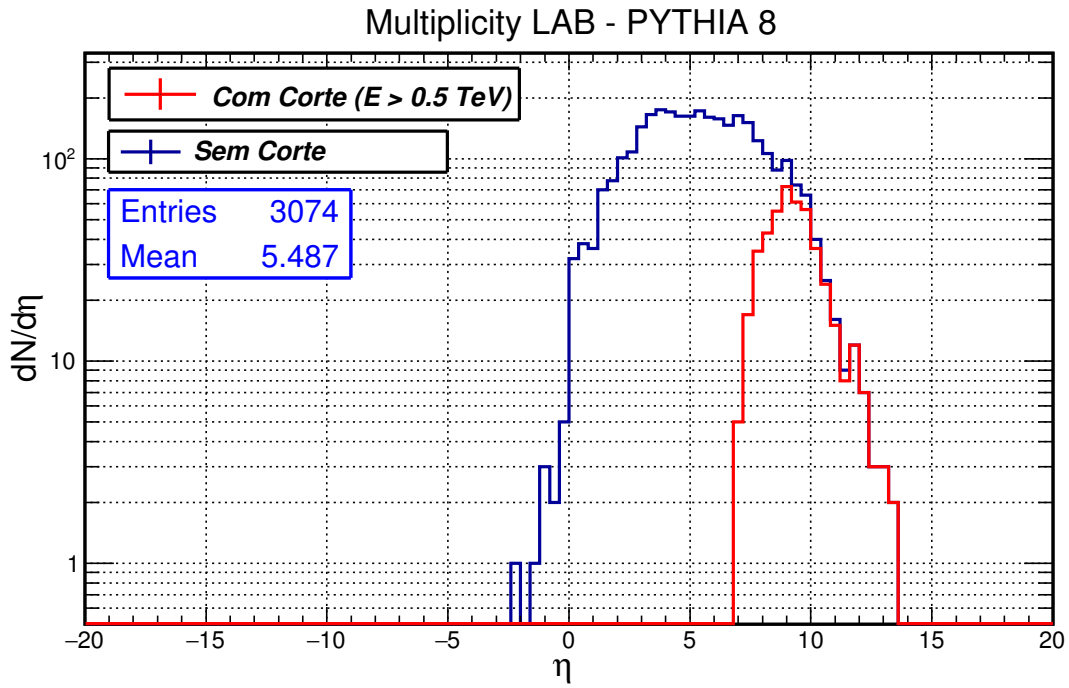

Figure 9: Distribution of particles as a function of the pseudo-rapidity in the LAB reference frame represented in the histograms without cut e with cut. A distribuição with cut represents an estimate of the events observed by CBJ in the emulsion chamber.

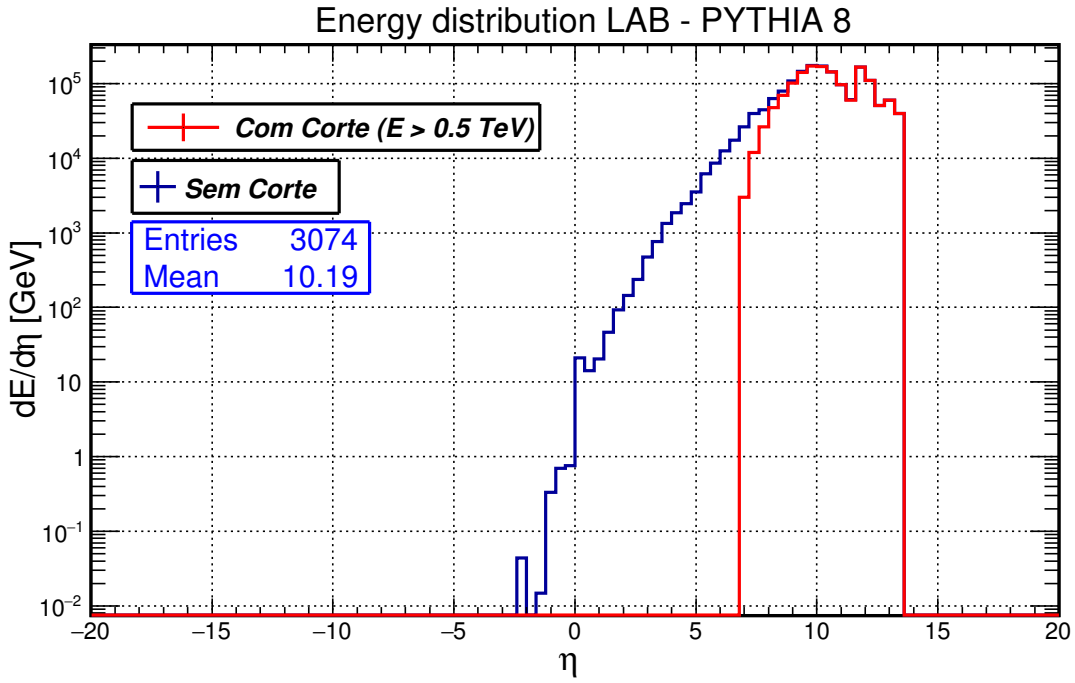

Figure 10: Energy distribution as a function of the pseudo-rapidity in the LAB reference frame represented in the histograms without cut and with cut. The Distribution with cut represents an estimate of the events observed by the CBJ in the emulsion chamber.

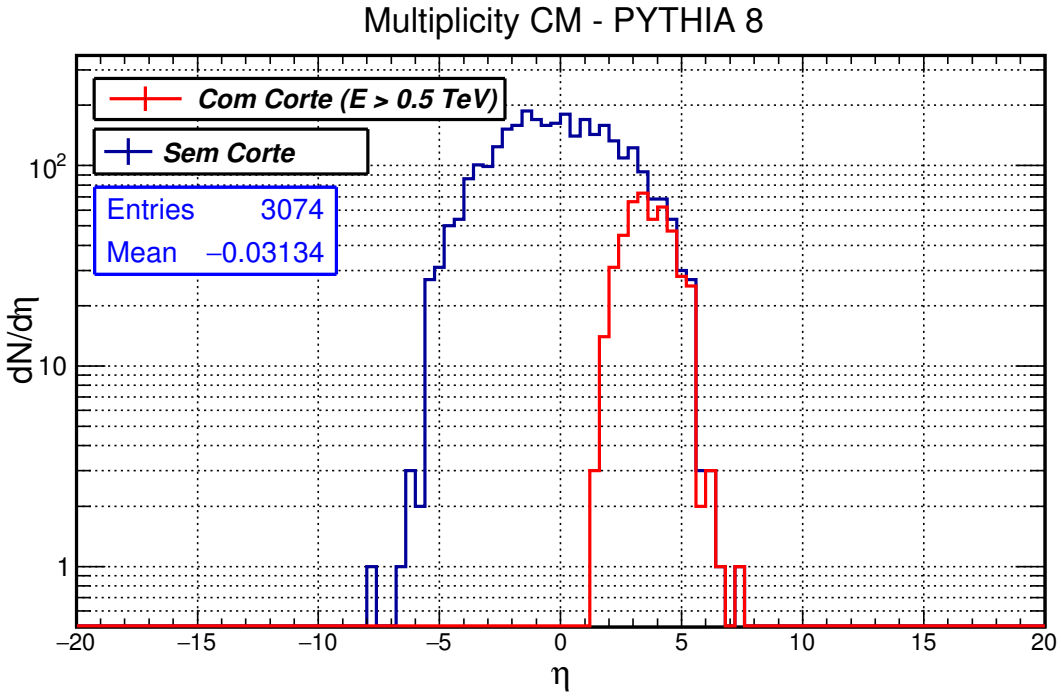

Figure 11: Distribution of particles as a function of the pseudo-rapidity in the CM reference frame represented in the histograms without cut e with cut. A distribuição with cut represents an estimate of the events observed by CBJ in the emulsion chamber.

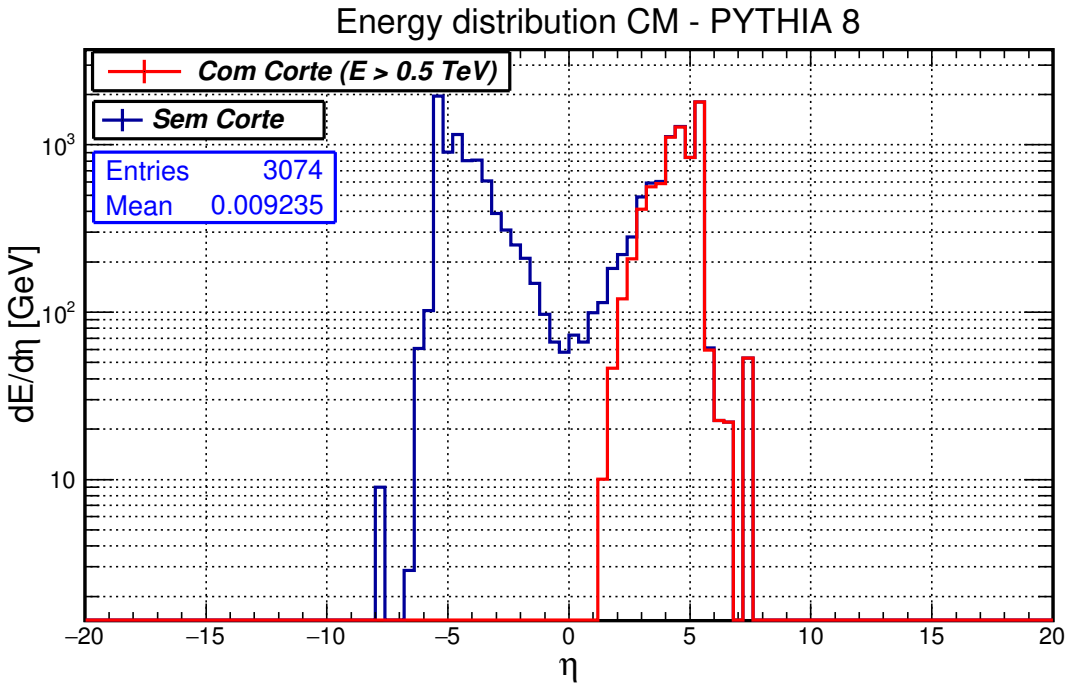

Figure 12: Energy distribution as a function of the pseudo-rapidity in the CM reference frame represented in the histograms without cut and with cut. The Distribution with cut represents an estimate of the events observed by the CBJ in the emulsion chamber.

9.1.2 $\mathbf{E_{LAB} = 80\ TeV \rightarrow \sqrt{s} = 387.46\ GeV}$

- 82 Colisões pp no referencilal do LAB (82 Eventos C-jatos), $E_{cut} = 0.5$ TeV.
- Beam 1 ($E_{BEAM\ 1} = 80$ TeV), Beam 2 ($E_{BEAM\ 2} = m_p$), $\gamma_{CM} = 206.4755$, $\beta_{CM} = 0.999976544$.
- $\sqrt{s} = \sqrt{2m_pE} = \sqrt{2 \cdot 0.9383 \cdot 80.10^3} = 387.4635$ GeV.

```
*-------  PYTHIA Event and Cross Section Statistics  ---------------*
| Subprocess                          events |      sigma +- delta       |
|                                            |    (estimated) (mb)       |
|-------------------------------------------------------------------------|
| non-diffractive                         55 |   3.149e+01  2.273e-07    |
| p p -> p p elastic                      11 |   1.076e+01  0.000e+00    |
| p p -> X p single diffractive            6 |   4.970e+00  3.441e-08    |
| p p -> p X single diffractive            5 |   4.970e+00  0.000e+00    |
| p p -> X X double diffractive            5 |   4.908e+00  0.000e+00    |
|-------------------------------------------------------------------------|
# sum                                      82 |   5.710e+01  2.299e-07    |
*-------  End PYTHIA Event and Cross Section Statistics -----------*
```

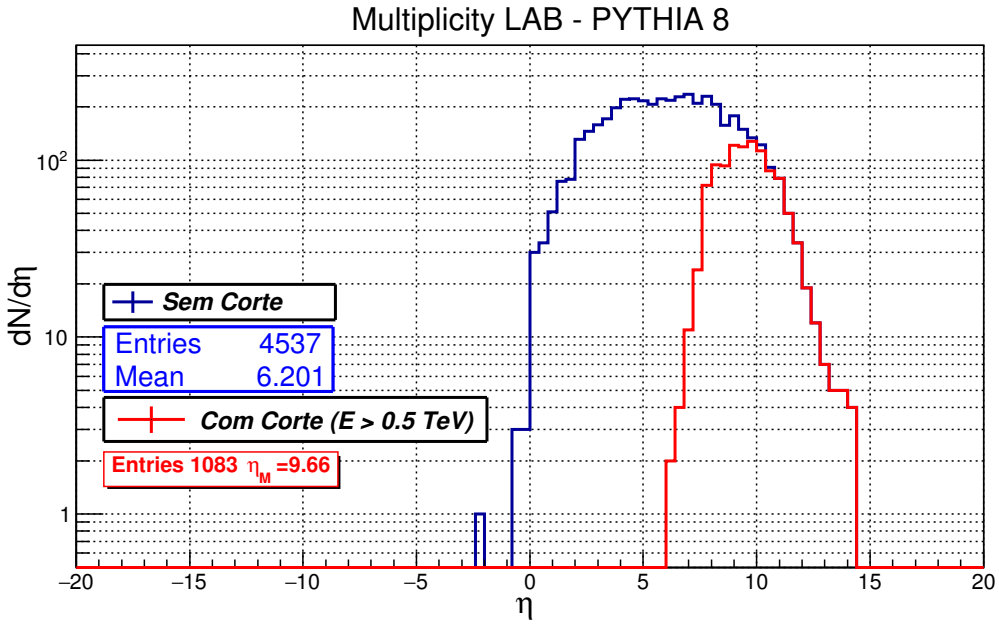

Figure 13: Distribution of particles as a function of the pseudo-rapidity in the LAB reference frame represented in the histograms without cut e with cut. A distribuição with cut represents an estimate of the events observed by CBJ in the emulsion chamber.

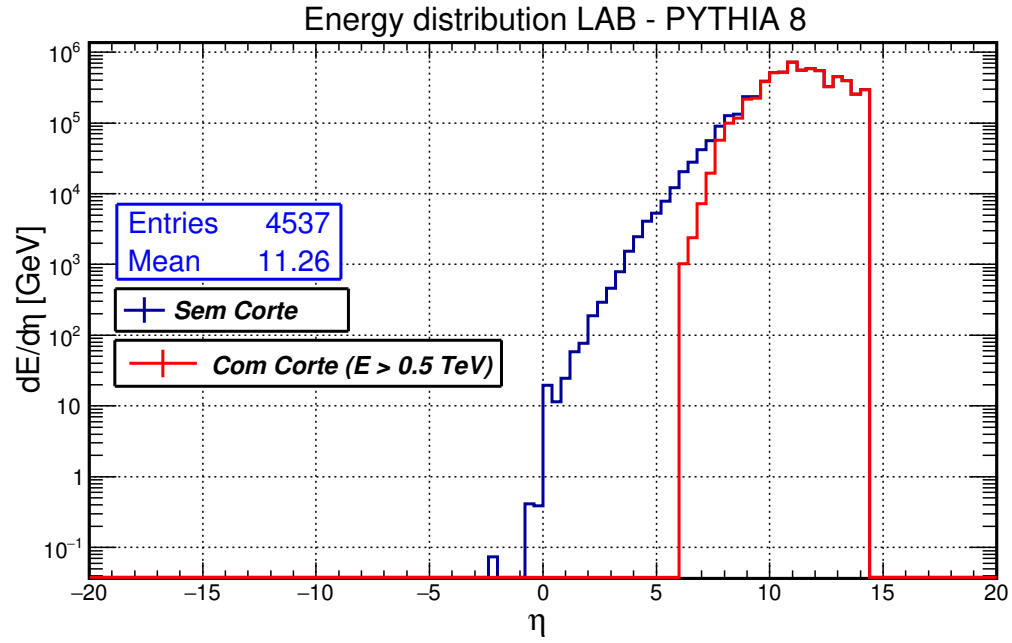

Figure 14: Energy distribution as a function of the pseudo-rapidity in the LAB reference frame represented in the histograms without cut and with cut. The Distribution with cut represents an estimate of the events observed by the CBJ in the emulsion chamber.

9.1.3 $\mathbf{E_{LAB} = 120\ TeV \rightarrow \sqrt{s} = 474.54\ GeV}$

- 82 Colisões pp no referencilal do LAB (82 Eventos C-jatos), $E_{cut} = 0.5$ TeV.

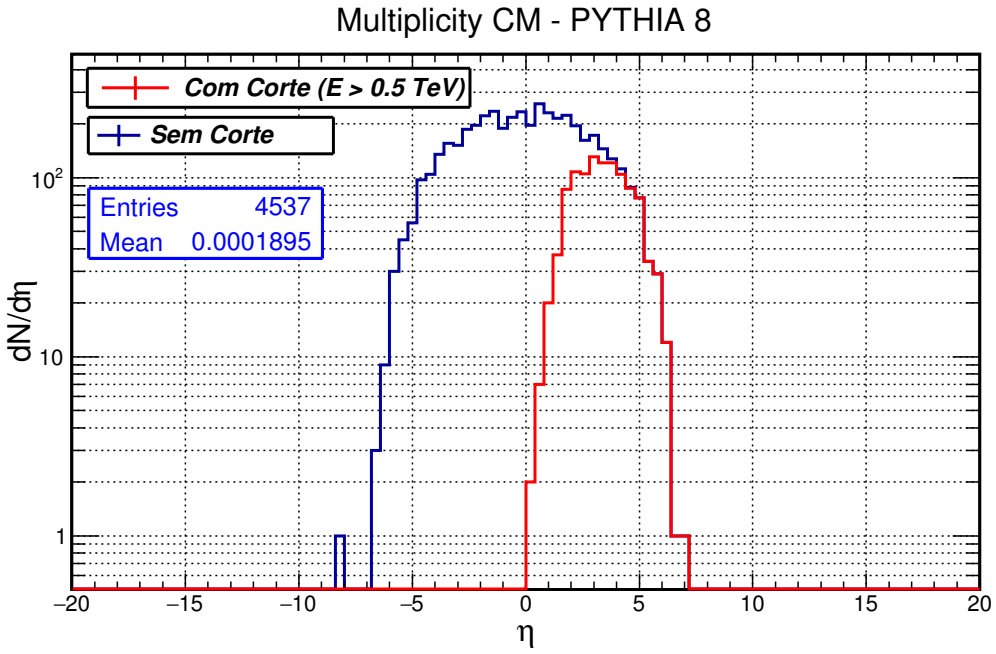

Figure 15: Distribution of particles as a function of the pseudo-rapidity in the CM reference frame represented in the histograms without cut e with cut. A distribuição with cut represents an estimate of the events observed by CBJ in the emulsion chamber.

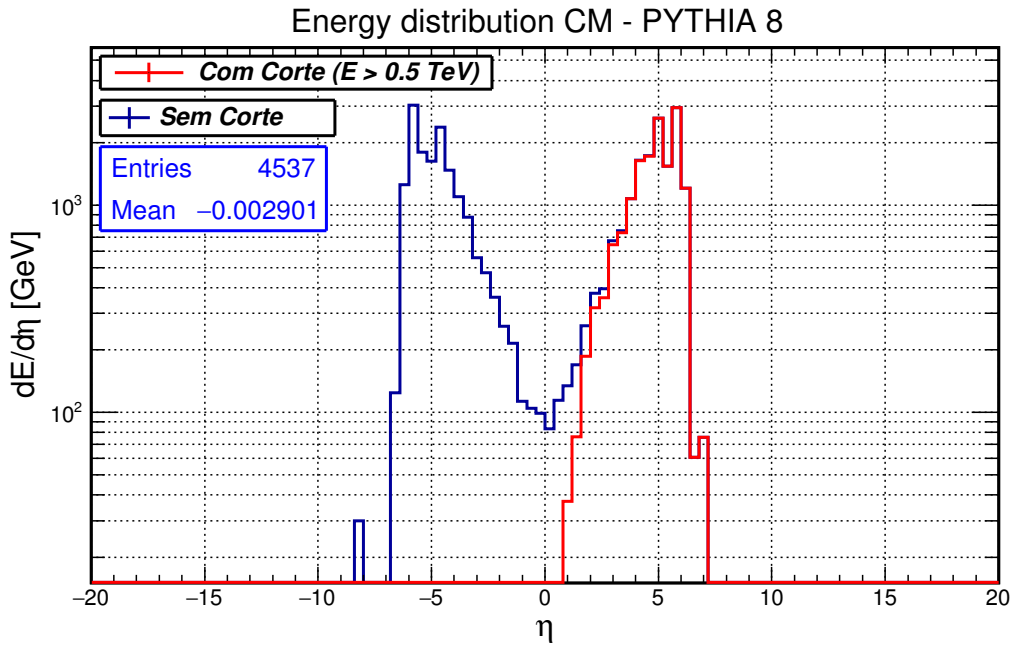

Figure 16: Energy distribution as a function of the pseudo-rapidity in the CM reference frame represented in the histograms without cut and with cut. The Distribution with cut represents an estimate of the events observed by the CBJ in the emulsion chamber.

- Beam 1 ($E_{BEAM\ 1} = 120$ TeV), Beam 2 ($E_{BEAM\ 2} = m_p$), $\gamma_{CM} = 252.8784$, $\beta_{CM} = 0.999992181$.
- $\sqrt{s} = \sqrt{2m_pE} = \sqrt{2 \cdot 0.9383 \cdot 120.10^3} = 474.54$ GeV.

```
*-------  PYTHIA Event and Cross Section Statistics  ---------------*
| Subprocess                          events |      sigma +- delta        |
|                                            |     (estimated) (mb)       |
|-------------------------------------------------------------------------|
| non-diffractive                        39 |   3.248e+01   1.707e-07    |
| p p -> p p elastic                     16 |   1.122e+01   5.162e-08    |
| p p -> X p single diffractive           9 |   5.066e+00   1.987e-08    |
| p p -> p X single diffractive           7 |   5.066e+00   0.000e+00    |
| p p -> X X double diffractive          11 |   5.127e+00   1.797e-08    |
|-------------------------------------------------------------------------|
# sum                                  82 |   5.895e+01     1.804e-07  |
*--------  End PYTHIA Event and Cross Section Statistics -----------*
```

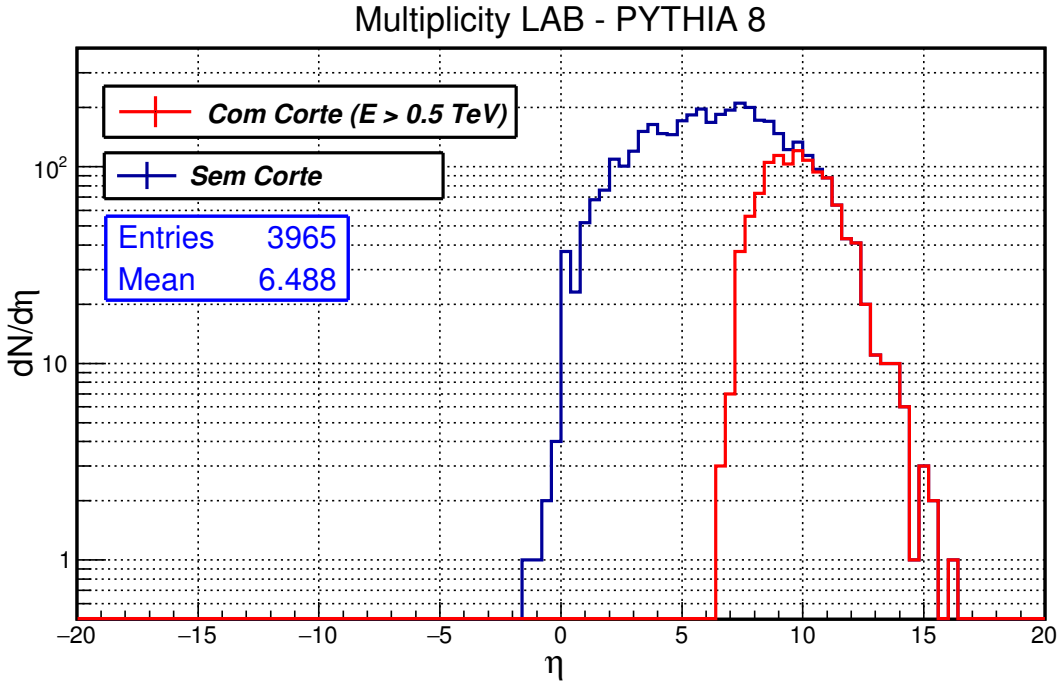

Figure 17: Distribution of particles as a function of the pseudo-rapidity in the LAB reference frame represented in the histograms without cut e with cut. A distribuição with cut represents an estimate of the events observed by CBJ in the emulsion chamber.

9.2 Single Diffractive

9.2.1 $\mathbf{E_{LAB} = 20\ TeV \rightarrow \sqrt{s} = 193.73\ GeV}$

- 200 Colisões pp no referencilal do LAB (82 Eventos C-jatos), $E_{cut} = 0.5$ TeV.
- Beam 1 ($E_{BEAM\ 1} = 20$ TeV), Beam 2 ($E_{BEAM\ 2} = m_p = 0.9383$ GeV), $\gamma_{CM} = 103.24$, $\beta_{CM} = 0.9999533089$.

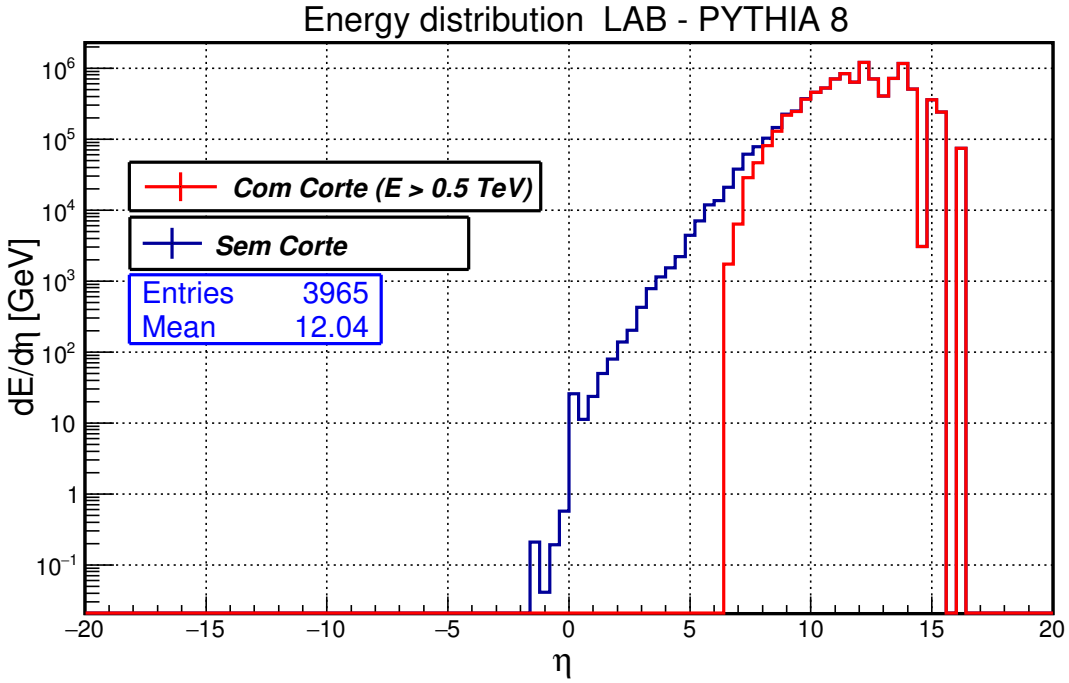

Figure 18: Energy distribution as a function of the pseudo-rapidity in the LAB reference frame represented in the histograms without cut and with cut. The Distribution with cut represents an estimate of the events observed by the CBJ in the emulsion chamber.

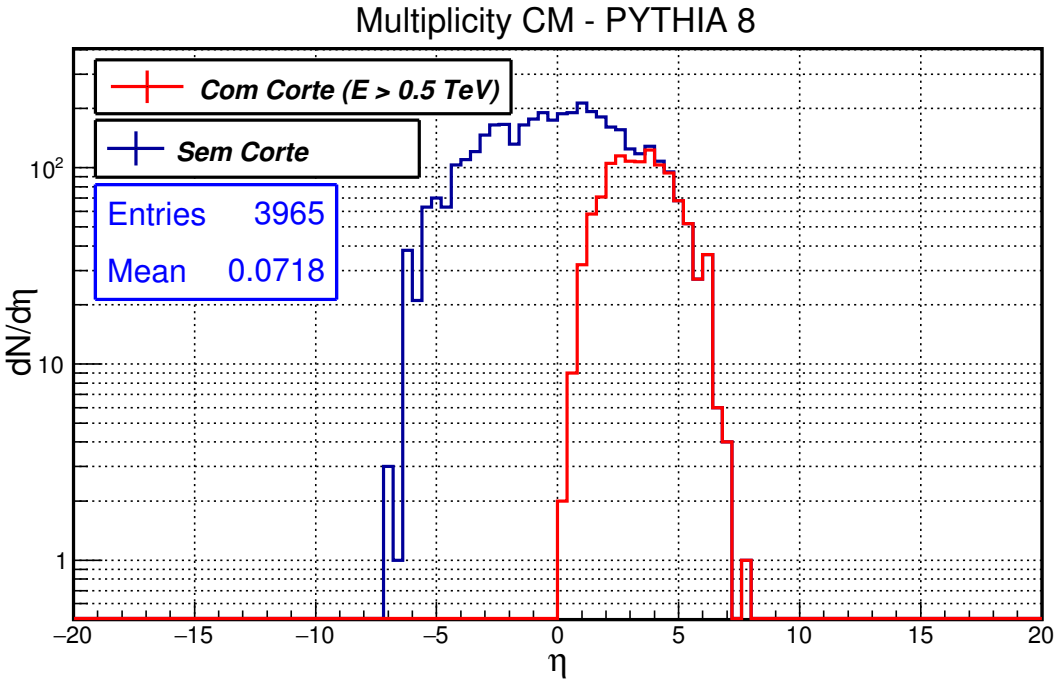

Figure 19: Distribution of particles as a function of the pseudo-rapidity in the CM reference frame represented in the histograms without cut e with cut. A distribuição with cut represents an estimate of the events observed by CBJ in the emulsion chamber.

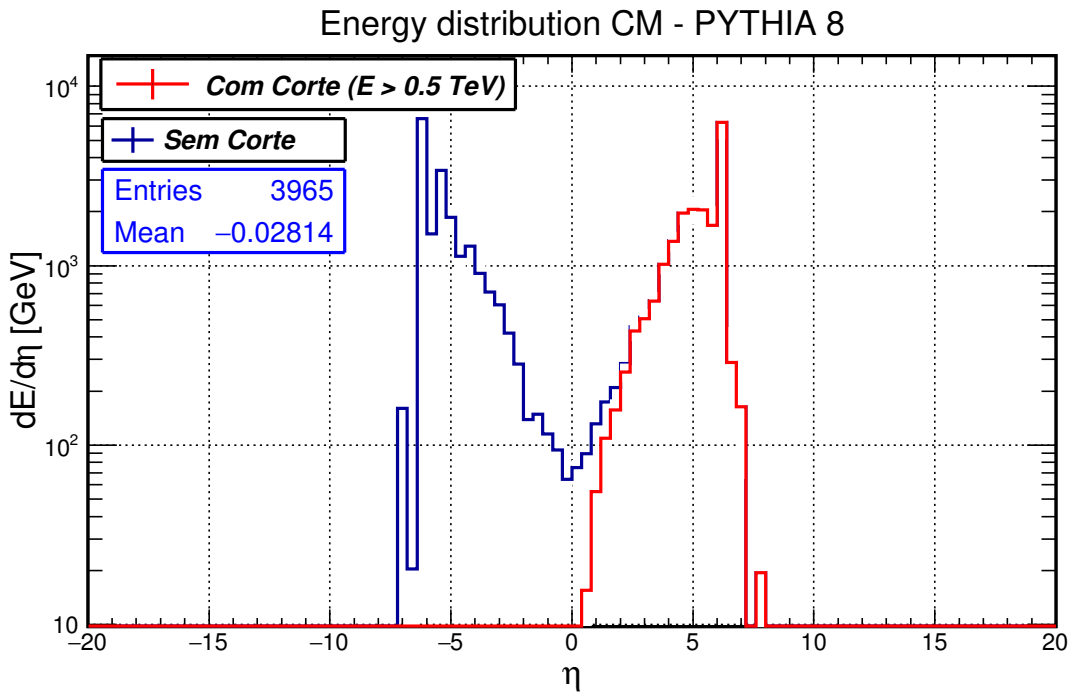

Figure 20: Energy distribution as a function of the pseudo-rapidity in the CM reference frame represented in the histograms without cut and with cut. The Distribution with cut represents an estimate of the events observed by the CBJ in the emulsion chamber.

- $\sqrt{s} = \sqrt{2\mathrm{m_p E}} = \sqrt{2 \cdot 0.9383 \cdot 20.10^3} = 193.73$ GeV.

```
*-------  PYTHIA Event and Cross Section Statistics  ---------------*
| Subprocess                          events |      sigma +- delta        |
|                                            |    (estimated) (mb)        |
|-------------------------------------------------------------------------|
| p p -> X p single diffractive         94 |   4.627e+00  3.074e-08     |
| p p -> p X single diffractive        106 |   4.627e+00  2.715e-08     |
|-------------------------------------------------------------------------|
# sum                                  200 |   9.255e+00  4.101e-08     |
*--------  End PYTHIA Event and Cross Section Statistics -----------*
```

9.2.2 $\mathbf{E_{LAB} = 120\ TeV \rightarrow \sqrt{s} = 474.54\ GeV}$

- 100 Colisões pp no referencilal do LAB (82 Eventos C-jatos), $\mathrm{E_{cut}} = 0.5$ TeV.
- Beam 1 ($\mathrm{E_{BEAM\ 1}} = 120$ TeV), Beam 2 ($\mathrm{E_{BEAM\ 2}} = \mathrm{m_p}$), $\gamma_{\mathrm{CM}} = 252.8784$, $\beta_{\mathrm{CM}} = 0.999992181$.
- $\sqrt{s} = \sqrt{2\mathrm{m_p E}} = \sqrt{2 \cdot 0.9383 \cdot 120.10^3} = 474.54$ GeV.

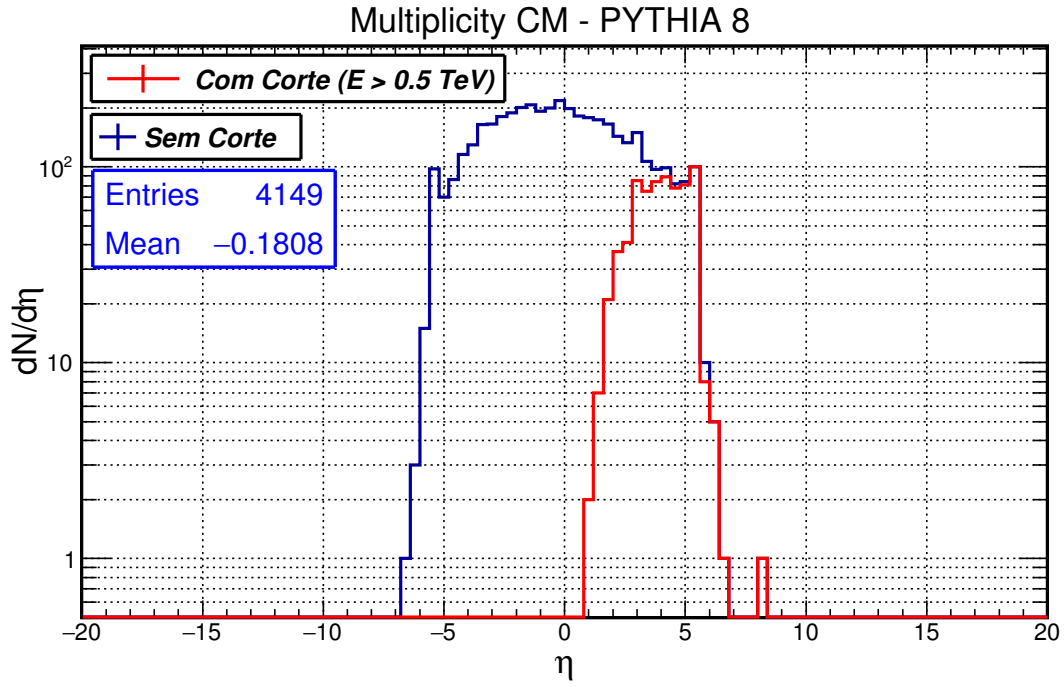

Figure 21: Distribution of particles as a function of the pseudo-rapidity in the CM reference frame represented in the histograms without cut e with cut. A distribuição with cut represents an estimate of the events observed by CBJ in the emulsion chamber.

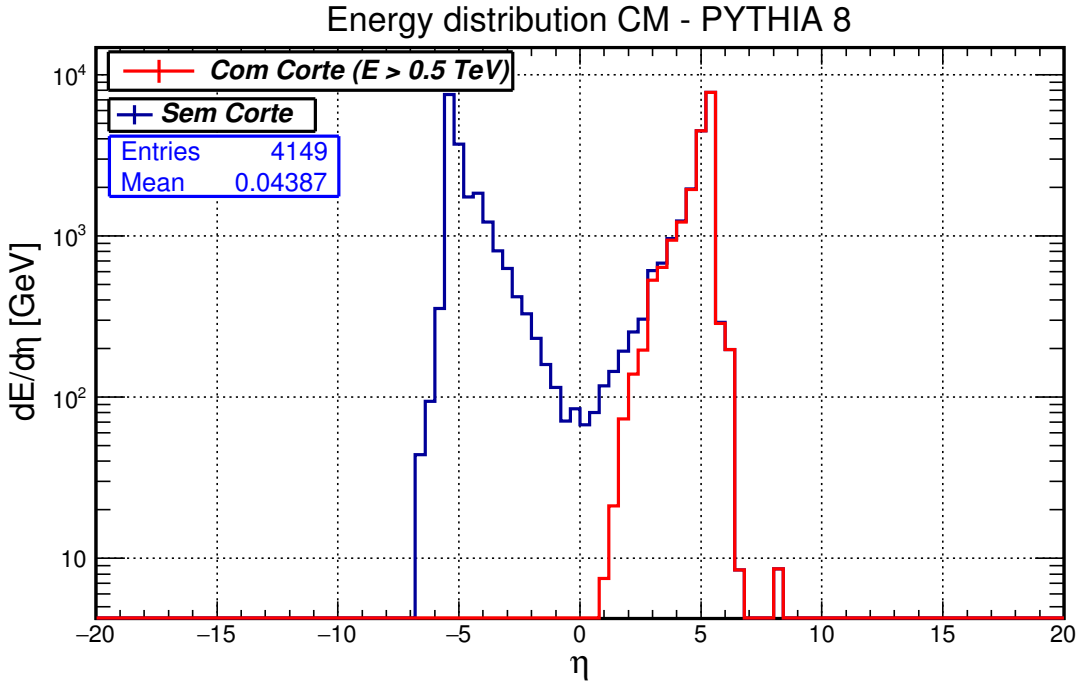

Figure 22: Energy distribution as a function of the pseudo-rapidity in the CM reference frame represented in the histograms without cut and with cut. The Distribution with cut represents an estimate of the events observed by the CBJ in the emulsion chamber.

```
*-------  PYTHIA Event and Cross Section Statistics  ---------------*
| Subprocess                          events |      sigma +- delta        |
|                                            |     (estimated) (mb)       |
|-------------------------------------------------------------------------|
| p p -> X p single diffractive         49 |   5.066e+00  0.000e+00      |
| p p -> p X single diffractive         51 |   5.066e+00  0.000e+00      |
|-------------------------------------------------------------------------|
# sum                                  100 |   1.013e+01  0.000e+00      |
*--------  End PYTHIA Event and Cross Section Statistics -----------*
```

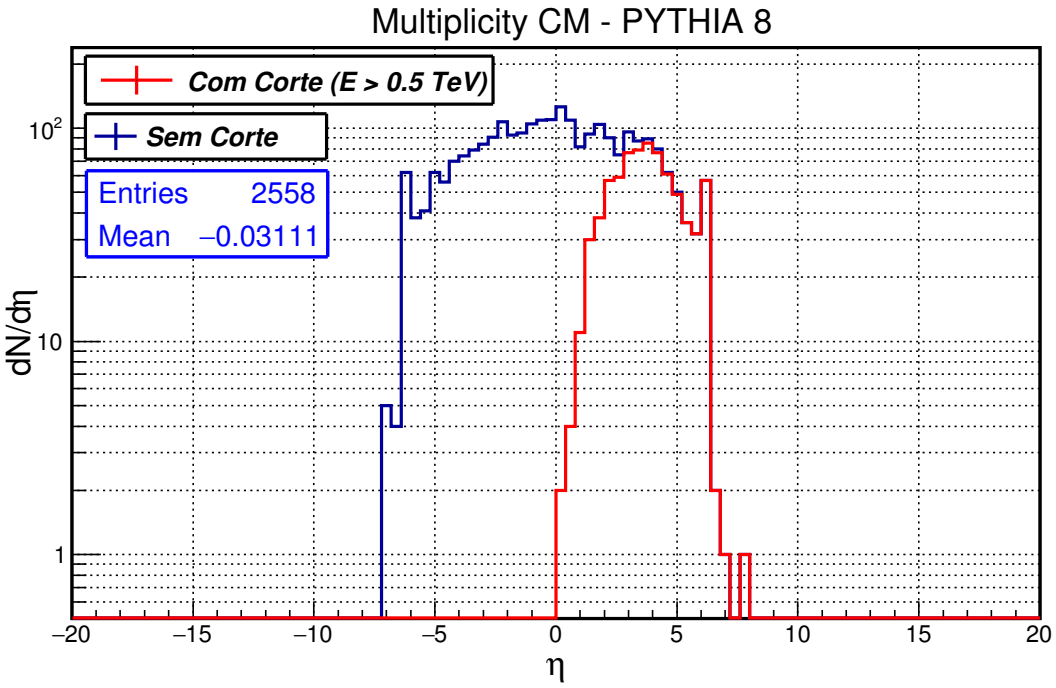

Figure 23: Distribution of particles as a function of the pseudo-rapidity in the CM reference frame represented in the histograms without cut e with cut. A distribuição with cut represents an estimate of the events observed by CBJ in the emulsion chamber.

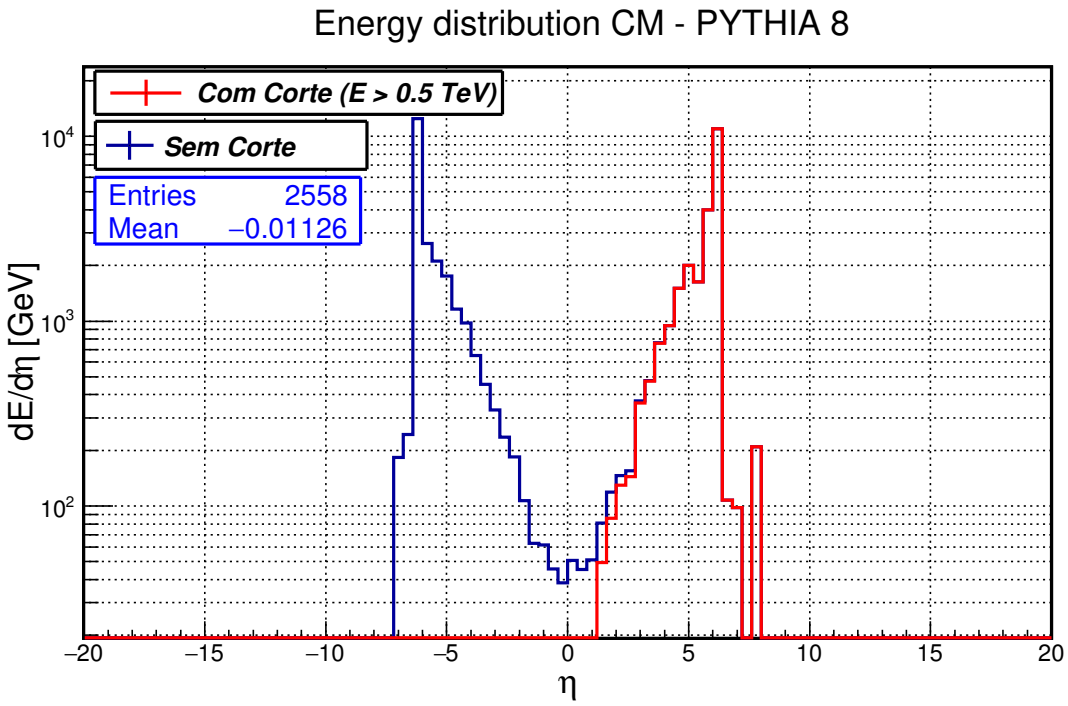

Figure 24: Energy distribution as a function of the pseudo-rapidity in the CM reference frame represented in the histograms without cut and with cut. The Distribution with cut represents an estimate of the events observed by the CBJ in the emulsion chamber.

9.3 Double Diffractive

9.3.1 $\mathbf{E_{LAB} = 20\ TeV \rightarrow \sqrt{s} = 193.73\ GeV}$

```
*-------  PYTHIA Event and Cross Section Statistics  ---------------*
| Subprocess                          events |      sigma +- delta        |
|                                            |     (estimated) (mb)       |
|-------------------------------------------------------------------------|
| p p -> X X double diffractive          100 |   4.167e+00  2.065e-08     |
|-------------------------------------------------------------------------|
# sum                                  100 |   4.167e+00  2.065e-08     |
*--------  End PYTHIA Event and Cross Section Statistics -----------*
```

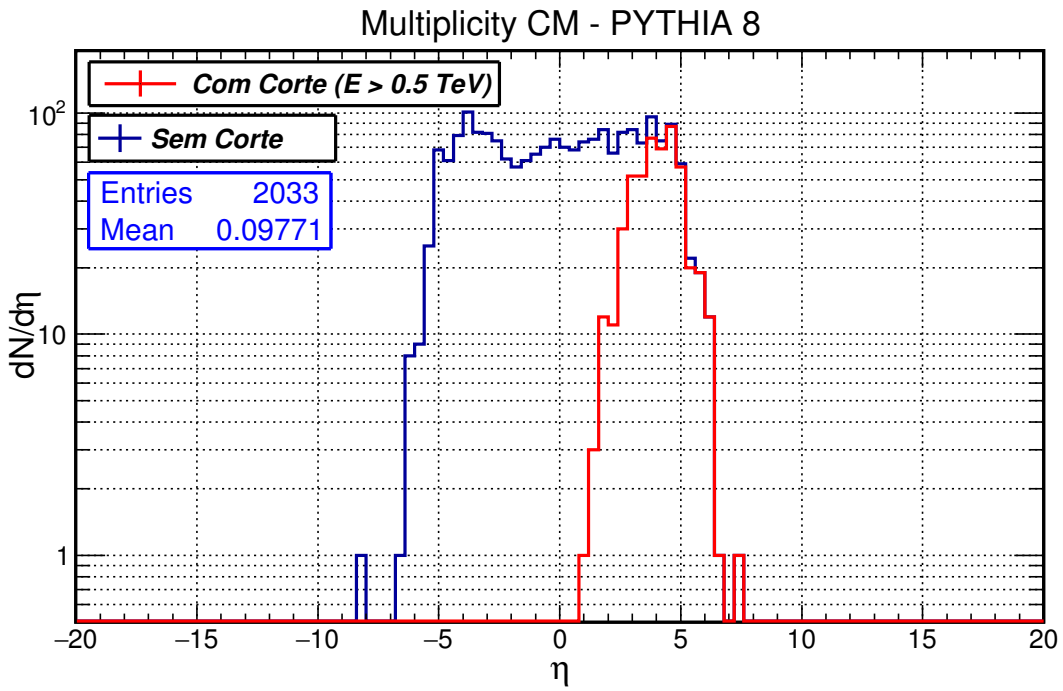

Figure 25: Distribution of particles as a function of the pseudo-rapidity in the CM reference frame represented in the histograms without cut e with cut. A distribuição with cut represents an estimate of the events observed by CBJ in the emulsion chamber.

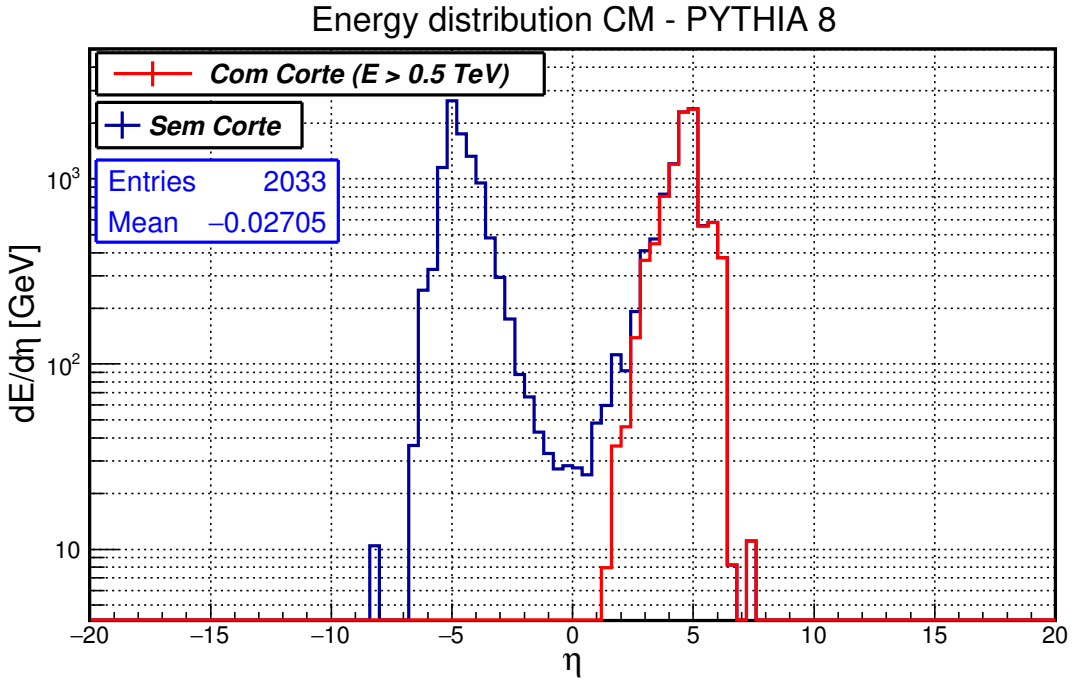

Figure 26: Energy distribution as a function of the pseudo-rapidity in the CM reference frame represented in the histograms without cut and with cut. The Distribution with cut represents an estimate of the events observed by the CBJ in the emulsion chamber.

9.3.2 $E_{LAB} = 120$ TeV $\rightarrow \sqrt{s} = 474.54$ GeV

```
*-------  PYTHIA Event and Cross Section Statistics  ---------------*
| Subprocess                          events |      sigma +- delta        |
|                                            |     (estimated) (mb)        |
|-------------------------------------------------------------------------|
| p p -> X X double diffractive          100 |   5.127e+00  2.920e-08      |
|-------------------------------------------------------------------------|
# sum                                  100 |   5.127e+00  2.920e-08      |
*--------  End PYTHIA Event and Cross Section Statistics -----------*
```

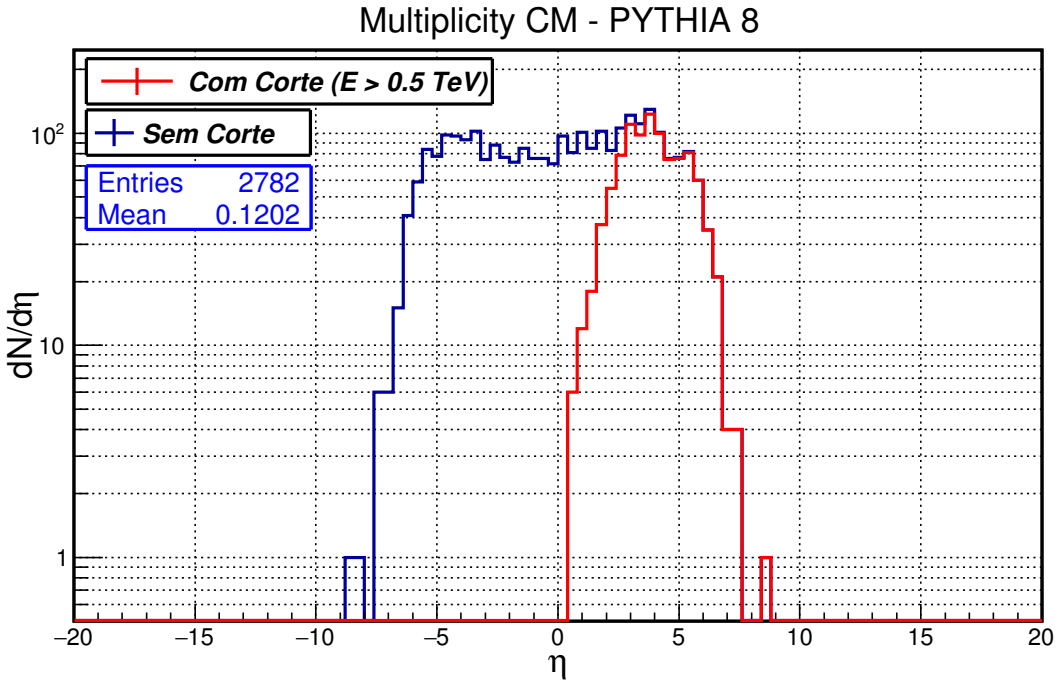

Figure 27: Distribution of particles as a function of the pseudo-rapidity in the CM reference frame represented in the histograms without cut e with cut. A distribuição with cut represents an estimate of the events observed by CBJ in the emulsion chamber.

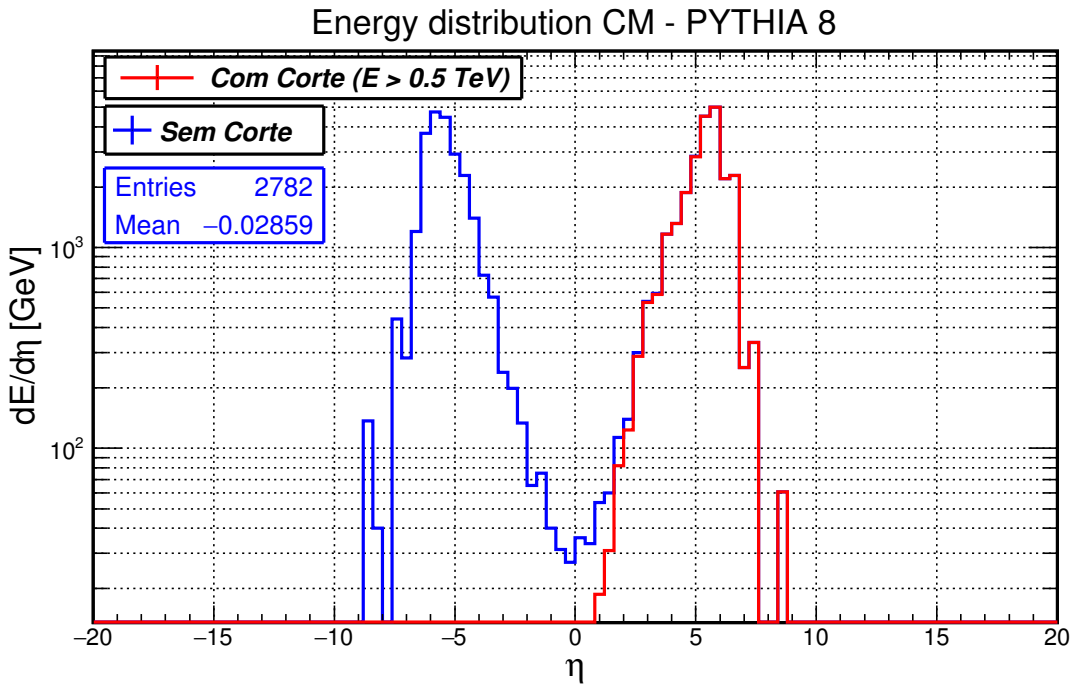

Figure 28: Energy distribution as a function of the pseudo-rapidity in the CM reference frame represented in the histograms without cut and with cut. The Distribution with cut represents an estimate of the events observed by the CBJ in the emulsion chamber.

9.4 HardQCD

- 1000 Colisões pp no referencilal do LAB (82 Eventos C-jatos), $E_{cut} = 0.5$ TeV.
- $p_{T\text{mín}} = 20$ GeV. (Esse parâmetro favorece a formação de jatos)
- Beam 1 ($E_{BEAM\ 1} = 120$ TeV), Beam 2 ($E_{BEAM\ 2} = m_p$), $\gamma_{CM} = 252.8784$, $\beta_{CM} = 0.999992181$, $\sqrt{s} = 474.54$ GeV

```
*-------  PYTHIA Event and Cross Section Statistics  ---------------*
| Subprocess                         events |      sigma +- delta (mb)   |
|-------------------------------------------------------------------------|
| gg -> gg                              333  |   4.416e-04  1.262e-05     |
| gg -> qqbar (uds)                       6  |   1.554e-05  2.453e-06     |
| qg -> qg                              495  |   7.186e-04  1.616e-05     |
| qq(bar)'->qq(bar)'                    158  |   2.385e-04  9.010e-06     |
| qqbar -> gg                             0  |   0.000e+00  0.000e+00     |
| qqbar -> q'qbar' (uds)                  2  |   2.973e-06  1.045e-06     |
| gg -> ccbar                             2  |   2.276e-06  6.517e-07     |
| qqbar -> ccbar                          1  |   1.998e-06  1.998e-06     |
| gg -> bbbar                             3  |   3.664e-06  1.608e-06     |
| qqbar -> bbbar                          0  |   0.000e+00  0.000e+00     |
# sum                                1000  |   1.425e-03  2.270e-05     |
*--------  End PYTHIA Event and Cross Section Statistics -----------*
```

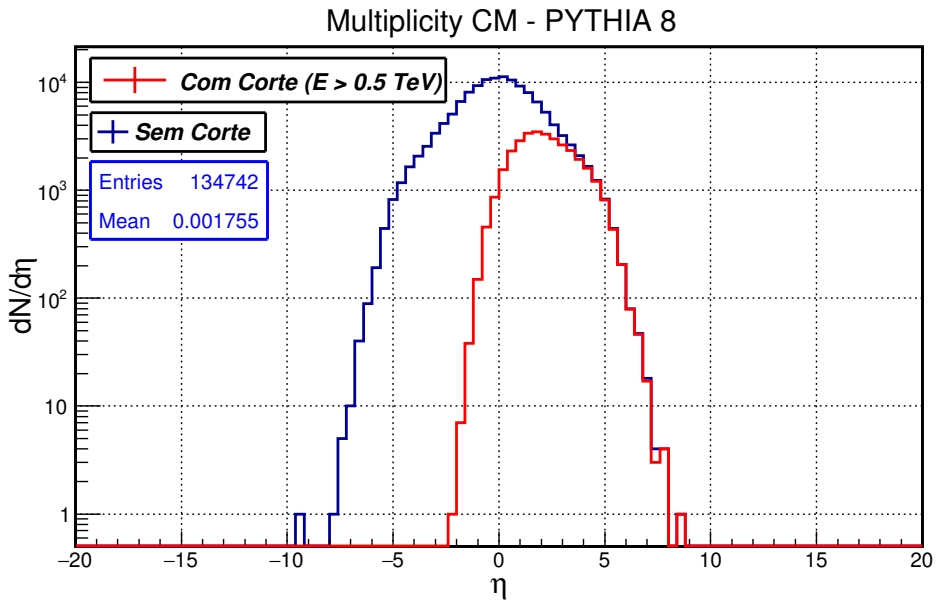

Figure 29: Distribution of particles as a function of the pseudo-rapidity in the CM reference frame represented in the histograms without cut e with cut. There is a noticeable difference in this distribution compared to softQCD in the central region ($|\eta| \leq 2$), whose difference can be attributed to the formation of jets.

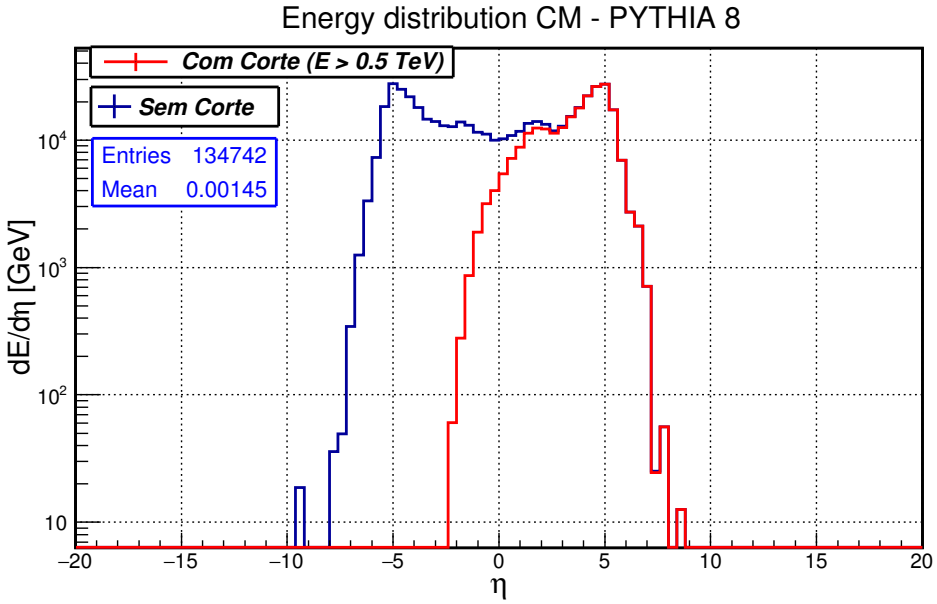

Figure 30: Energy distribution as a function of the pseudo-rapidity in the CM reference frame represented in the histograms without cut and with cut. There is a noticeable difference in this distribution compared to softQCD in the central region ($|\eta| \leq 2$), "SIGNAL", whose difference can be attributed to the formation of jets.

10 The CBJ Data is Compared to Prediction from the PYTHIA 8 Event Generator

- 110 pp collisions in LAB referencilal (82 C-jet events), $E_{cut} = 0.5$ TeV.
- Beam 1 ($E_{BEAM\ 1} = 80$ TeV), Beam 2 ($E_{BEAM\ 2} = m_p$), $\gamma_{CM} = 206.4755$, $\beta_{CM} = 0.999976544$.
- $\sqrt{s} = 387.4635$ GeV.
- According to the CBJ data (see Table 3) the majority of the events have energy in the range of 20 - 30 TeV (25 TeV) ($\sim 1/3$ of the initial energy (E_0) the event, i.e., $E_0 = 75$ TeV).
- In reference [52] is setting a maximum value for speed $y_{max} = 12.2$, with the observable phase space $y_\gamma \geq 7$.

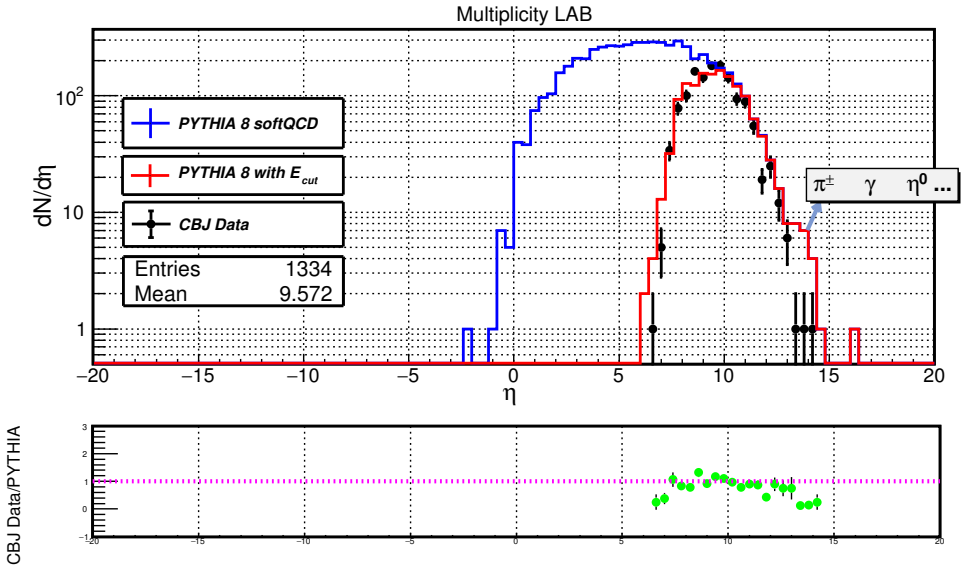

Figure 31: Distribution of particles as a function of the pseudo-rapidity in the LAB reference frame represented in the histograms without cut e with cut. A distribuição with cut represents an estimate of the events observed by CBJ in the emulsion chamber.

Lorentz Transformation

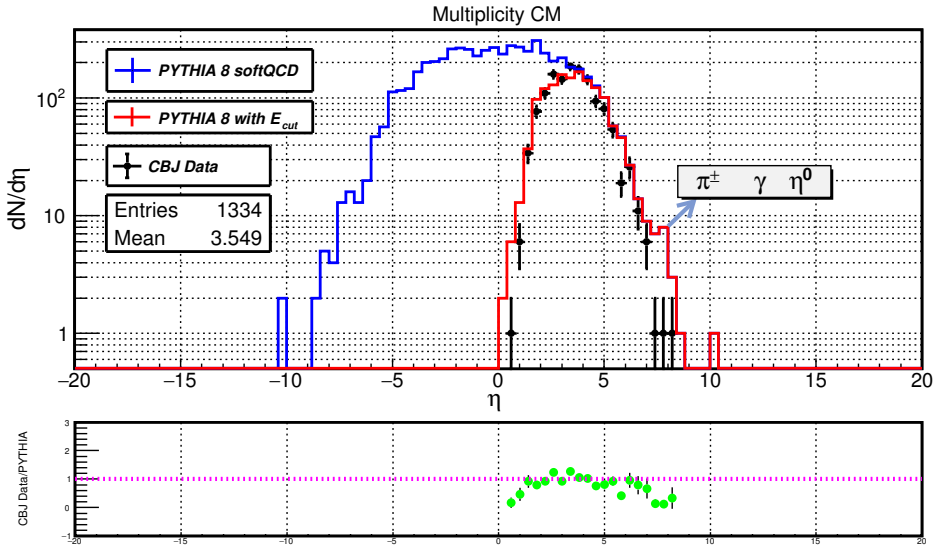

Figure 32: Distribution of particles as a function of the pseudo-rapidity in the CM reference frame represented in the histograms without cut e with cut. A distribuição with cut represents an estimate of the events observed by CBJ in the emulsion chamber.

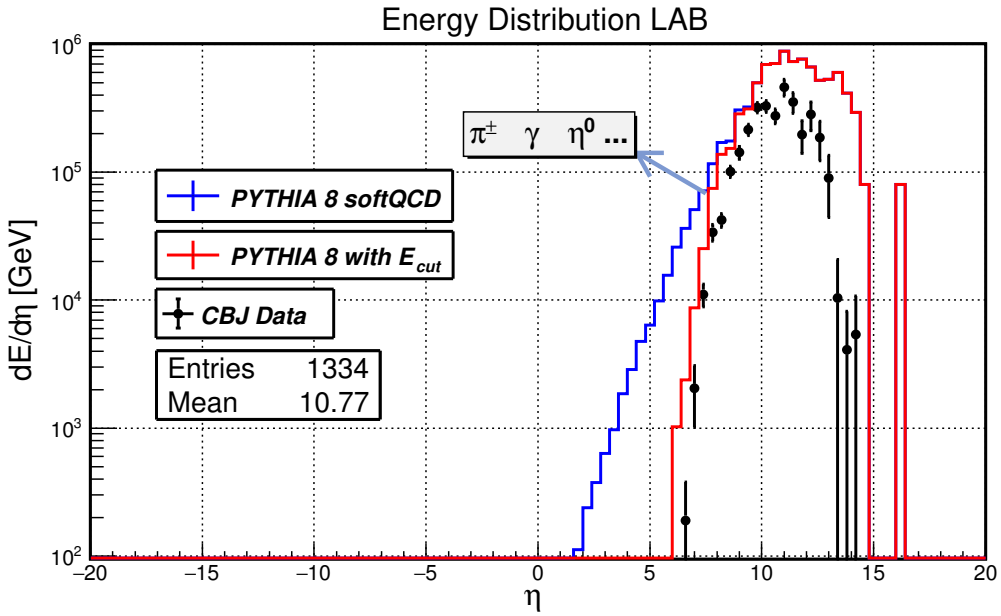

Figure 33: Energy distribution as a function of the pseudo-rapidity in the CM reference frame represented in the histograms without cut and with cut. The Distribution with cut represents an estimate of the events observed by the CBJ in the emulsion chamber.

References

[1]M. T. Dova, "Ultra-High Energy Cosmic Rays", in Proceedings, 7th CERN–Latin-American School of High-Energy Physics (CLASHEP2013): Arequipa, Peru, March 6-19, 2013 (2015), pp. 169–190.

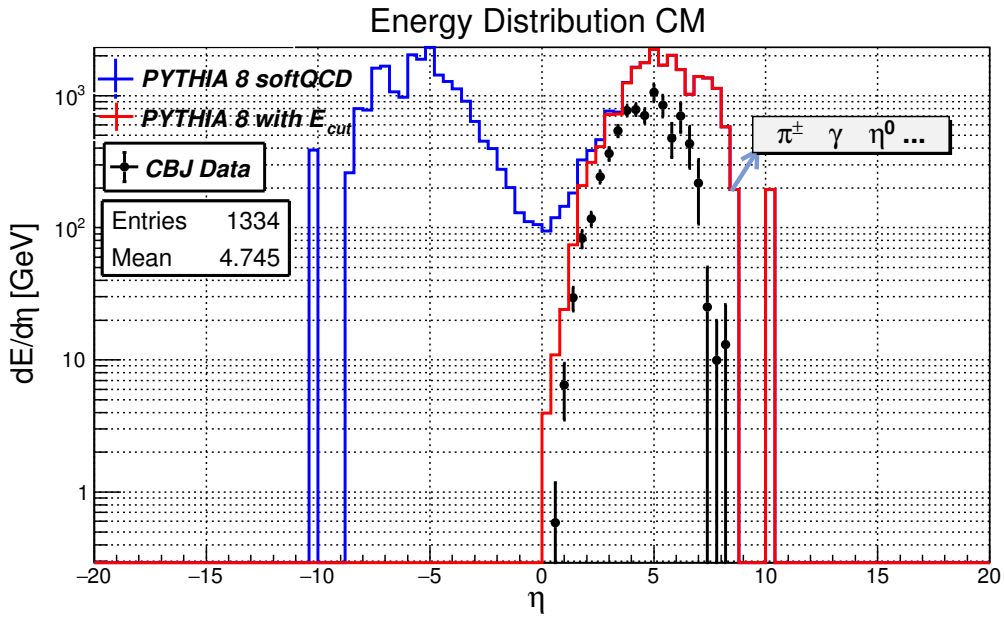

Figure 34: Energy distribution as a function of the pseudo-rapidity in the CM reference frame represented in the histograms without cut and with cut. The Distribution with cut represents an estimate of the events observed by the CBJ in the emulsion chamber.

[2]A. Haungs et al., "KCDC - The KASCADE Cosmic-ray Data Centre", J. Phys. Conf. Ser. **632**, 012011 (2015).

[3]C. M. Lattes, M. S. Mantovani, C. Santos, E. H. Shibuya, A. Turtelli, N. M. Amato, A. M. Endler, M. A. Bravo, C. Aguirre, M. Akashi, et al., "Chacaltaya emulsion chamber experiment", Progress of Theoretical Physics Supplement **47**, 1–125 (1971).

[4]M. Ballester et al., "COSMIC RAY OBSERVATION OF MULTIPLE PION PRODUCTION AT AROUND 100-TeV", Submitted to: Phys. Rev. (1981).

[5]J. Linsley, "Evidence for a primary cosmic-ray particle with energy 1020 ev", Physical Review Letters **10**, 146 (1963).

[6]T. Sjöstrand, S. Ask, J. R. Christiansen, R. Corke, N. Desai, P. Ilten, S. Mrenna, S. Prestel, C. O. Rasmussen, and P. Z. Skands, "An Introduction to PYTHIA 8.2", Comput. Phys. Commun. **191**, 159–177 (2015).

[7]T. Pierog, I. Karpenko, J. M. Katzy, E. Yatsenko, and K. Werner, "EPOS LHC: Test of collective hadronization with data measured at the CERN Large Hadron Collider", Phys. Rev. **C92**, 034906 (2015).

[8]D. d'Enterria, R. Engel, T. Pierog, S. Ostapchenko, and K. Werner, "Constraints from the first LHC data on hadronic event generators for ultra-high energy cosmic-ray physics", Astropart. Phys. **35**, 98–113 (2011).

[9]D. d'Enterria, R. Engel, T. McCauley, and T. Pierog, "Cosmic-ray Monte Carlo predictions for forward particle production in p-p, p-Pb, and Pb-Pb collisions at the LHC", Indian J. Phys. **84**, 1837–1842 (2010).

[10]D. G. d'Enterria, "Forward Physics at the LHC", in Proceedings, 15th International Workshop on Deep-inelastic scattering and related subjects (DIS 2007). Vol. 1 and 2: Munich, Germany, April 16-20, 2007 (2007), pp. 1141–1152.

[11]L. W. Jones, "Comparison of accelerator and cosmic ray data", Nuclear Physics B - Proceedings Supplements **75**, 54–61 (1999).

[12]M. Cacciari, G. P. Salam, and G. Soyez, "The anti-k_t jet clustering algorithm", Journal of High Energy Physics **2008**, 063 (2008).

[13]M. Cacciari, G. P. Salam, and G. Soyez, "Fastjet user manual", The European Physical Journal C **72**, 1896 (2012).

[14]S. Sapeta, "QCD and Jets at Hadron Colliders", Prog. Part. Nucl. Phys. **89**, 1–55 (2016).

[15]R. K. Ellis, W. J. Stirling, and B. R. Webber, *Qcd and collider physics* (Cambridge university press, 2003).

[16]C. Loizides, "Glauber modeling of high-energy nuclear collisions at the subnucleon level", Phys. Rev. C **94**, 024914 (2016).

[17]G. Aad et al., "Measurement of the centrality dependence of the charged-particle pseudorapidity distribution in proton–lead collisions at $\sqrt{s_{\mathrm{NN}}} = 5.02$ TeV with the ATLAS detector", Eur. Phys. J. **C76**, 199 (2016).

[18]C. Bierlich, G. Gustafson, and L. Lönnblad, "Diffractive and non-diffractive wounded nucleons and final states in pA collisions", JHEP **10**, 139 (2016).

[19]H. J. Drescher, M. Hladik, S. Ostapchenko, T. Pierog, and K. Werner, "Parton based Gribov-Regge theory", Phys. Rept. **350**, 93–289 (2001).

[20]T. Pierog and K. Werner, "EPOS Model and Ultra High Energy Cosmic Rays", Nucl. Phys. Proc. Suppl. **196**, 102–105 (2009).

[21]E.-J. Ahn, R. Engel, T. K. Gaisser, P. Lipari, and T. Stanev, "Cosmic ray interaction event generator sibyll 2.1", Phys. Rev. D **80**, 094003 (2009).

[22]S. Ostapchenko, "Monte carlo treatment of hadronic interactions in enhanced pomeron scheme: qgsjet-ii model", Phys. Rev. D **83**, 014018 (2011).

[23]G. Aad et al., "The ATLAS Experiment at the CERN Large Hadron Collider", JINST **3**, S08003 (2008).

[24]K. Aamodt et al., "The ALICE experiment at the CERN LHC", JINST **3**, S08002 (2008).

[25]S. Chatrchyan et al., "The CMS experiment at the CERN LHC", JINST **3**, S08004 (2008).

[26]A. A. Alves Jr. et al., "The LHCb Detector at the LHC", JINST **3**, S08005 (2008).

[27]A. Buckley, J. Butterworth, L. Lonnblad, D. Grellscheid, H. Hoeth, J. Monk, H. Schulz, and F. Siegert, "Rivet user manual", Comput. Phys. Commun. **184**, 2803–2819 (2013).

[28]H. Kumano, "ANALYSES OF C JETS OBSERVED BY CHACALTAYA EMULSION CHAMBER", Prog. Theor. Phys. Suppl. **76**, 51–82 (1983).

[29]M. Thomson, *Modern particle physics* (Cambridge University Press, 2013).

[30]T. Schörner-Sadenius, *The large hadron collider: harvest of run 1* (Springer, 2015).

[31]K. A. Olive, P. D. Group, et al., "Review of particle physics", Chinese Physics C **38**, 090001 (2014).

[32]V. Gribov, Y. Dokshitzer, and J. Nyiri, "Strong interactions of hadrons at high energies", Gribov Lectures on Theoretical Physics (Cambridge University Press, Cambridge, United Kingdom, 2001) (2009).

[33]E. ZEIDLER, *Quantum field theory i: basics in mathematics and physics* (SPRINGER, 2016).

[34]A. Deur, S. J. Brodsky, and G. F. de Teramond, "The QCD Running Coupling", Prog. Part. Nucl. Phys. **90**, 1–74 (2016).

[35]A. Buckley et al., "General-purpose event generators for LHC physics", Phys. Rept. **504**, 145–233 (2011).

[36]G. Aad et al., "Properties of jets measured from tracks in proton-proton collisions at center-of-mass energy $\sqrt{s} = 7$ TeV with the ATLAS detector", Phys. Rev. **D84**, 054001 (2011).

[37]A. Donnachie and P. Landshoff, "Total cross sections", Physics Letters B **296**, 227–232 (1992).

[38]M. Deile et al., "Diffraction and total cross-section at the Tevatron and the LHC", Springer Proc. Phys. **108**, 40–45 (2006).

[39]P. Skands, "Introduction to QCD", in *Proceedings, Theoretical Advanced Study Institute in Elementary Particle Physics: Searching for New Physics at Small and Large Scales (TASI 2012): Boulder, Colorado, June 4-29, 2012*, [,63(2107)] (2013), pp. 341–420.

[40]K. Rabbertz, "Jet Physics at the LHC", Springer Tracts Mod. Phys. **268**, pp.1–214 (2017).

[41]V. Khachatryan et al., "The CMS trigger system", JINST **12**, P01020 (2017).

[42]M. Kaur and R. Gupta, "Parton level study of high ET jets in hard QCD processes at LHC", (2016).

[43]V. Khachatryan et al., "Production of leading charged particles and leading charged-particle jets at small transverse momenta in pp collisions at $\sqrt{s}$= 8 TeV", Phys. Rev. D **92**, 112001 (2015).

[44]S. Ganguly and M. Guchait, "Jet Cross-Section Measurements In CMS", Int. J. Mod. Phys. **A28**, 1330030 (2013).

[45]M. Cacciari, G. P. Salam, and G. Soyez, "The Anti-k(t) jet clustering algorithm", JHEP **04**, 063 (2008).

[46]S. Ostapchenko, "On the model dependence of the relation between minimum-bias and inelastic proton-proton cross sections", Phys. Lett. **B703**, 588–592 (2011).

[47]B. Abelev et al., "Measurement of inelastic, single- and double-diffraction cross sections in proton–proton collisions at the LHC with ALICE", Eur. Phys. J. **C73**, 2456 (2013).

[48]G. Aad et al., "Rapidity gap cross sections measured with the ATLAS detector in pp collisions at $\sqrt{s} = 7$ TeV", Eur. Phys. J. **C72**, 1926 (2012).

[49]S. Chatrchyan et al., "Measurement of pseudorapidity distributions of charged particles in proton-proton collisions at $\sqrt{s} = 8$ TeV by the CMS and TOTEM experiments", Eur. Phys. J. **C74**, 3053 (2014).

[50]R. D. Parsons, C. Bleve, S. S. Ostapchenko, and J. Knapp, "Systematic uncertainties in air shower measurements from high-energy hadronic interaction models", Astropart. Phys. **34**, 832–839 (2011).

[51]G. Pancheri and Y. N. Srivastava, "Introduction to the physics of the total cross-section at LHC", Eur. Phys. J. **C77**, 150 (2017).

[52]A. Ohsawa, "Study of nuclear interactions by emulsion chambers at Mt. Chacaltaya", Nucl. Phys. Proc. Suppl. **97**, [,16(2000)], 16–34 (2001).

[53]C.-Y. Wong, *Introduction to high-energy heavy-ion collisions* (World scientific, 1994).

[54]T. Söjstrand and M. van Zijl, "A Multiple Interaction Model for the Event Structure in Hadron Collisions", Phys. Rev. **D36**, 2019 (1987).

A Kinematic Relativistic

Lorentz Transformation LAB $\rightarrow$ CM

$$\begin{bmatrix} \mathrm{E}^* \\ \mathrm{p}_\mathrm{x}^* \\ \mathrm{p}_\mathrm{y}^* \\ \mathrm{p}_\mathrm{z}^* \end{bmatrix} = \begin{bmatrix} \gamma & -\beta_\mathrm{x}\gamma & -\beta_\mathrm{y}\gamma & -\beta_\mathrm{z}\gamma \\ -\beta_\mathrm{x}\gamma & 1+(\gamma-1)\frac{\beta_\mathrm{x}^2}{\beta^2} & (\gamma-1)\frac{\beta_\mathrm{x}\beta_\mathrm{y}}{\beta^2} & (\gamma-1)\frac{\beta_\mathrm{x}\beta_\mathrm{z}}{\beta^2} \\ -\beta_\mathrm{y}\gamma & (\gamma-1)\frac{\beta_\mathrm{y}\beta_\mathrm{x}}{\beta^2} & 1+(\gamma-1)\frac{\beta_\mathrm{y}^2}{\beta^2} & (\gamma-1)\frac{\beta_\mathrm{y}\beta_\mathrm{z}}{\beta^2} \\ -\beta_\mathrm{z}\gamma & (\gamma-1)\frac{\beta_\mathrm{z}\beta_\mathrm{x}}{\beta^2} & (\gamma-1)\frac{\beta_\mathrm{z}\beta_\mathrm{y}}{\beta^2} & 1+(\gamma-1)\frac{\beta_\mathrm{z}^2}{\beta^2} \end{bmatrix} \begin{bmatrix} \mathrm{E} \\ \mathrm{p}_\mathrm{x} \\ \mathrm{p}_\mathrm{y} \\ \mathrm{p}_\mathrm{z} \end{bmatrix}$$

Highly Relativistic Particles, $y \simeq \eta$

$$\gamma = \frac{1}{\sqrt{1-\beta^2}} \qquad \vec{\beta} = (\beta_\mathrm{x}, \beta_\mathrm{y}, \beta_\mathrm{z}) = \left(\frac{v_\mathrm{x}}{c}, \frac{v_\mathrm{y}}{c}, \frac{v_\mathrm{z}}{c}\right) = \frac{\vec{v}}{c}, \quad y \equiv \frac{1}{2}\ln\left[\frac{E+p_z}{E-p_z}\right] \simeq \eta$$

$$\mathrm{p_T} = \sqrt{\mathrm{p_x^2} + \mathrm{p_y^2}}, \quad \theta^* = \tan^{-1}\left(\frac{\mathrm{p_T}}{\mathrm{p_z^*}}\right), \quad \eta_\mathrm{CM} = -\ln\left[\tan\left(\frac{\theta^*}{2}\right)\right], \quad \eta_\mathrm{CM} = \eta_\mathrm{LAB} - \frac{1}{2}\ln\left[\frac{1+\beta}{1-\beta}\right]$$

$$\boxed{\mathrm{p_T} = \mathrm{p_T^*} \qquad \phi = \phi^* \qquad \sum_{i=1}^{N} \vec{\mathrm{p}}_i{}^* = \vec{0} \qquad \sum_{i=1}^{N} \mathrm{E}_i^* = \sqrt{\mathrm{s}}} \tag{9}$$

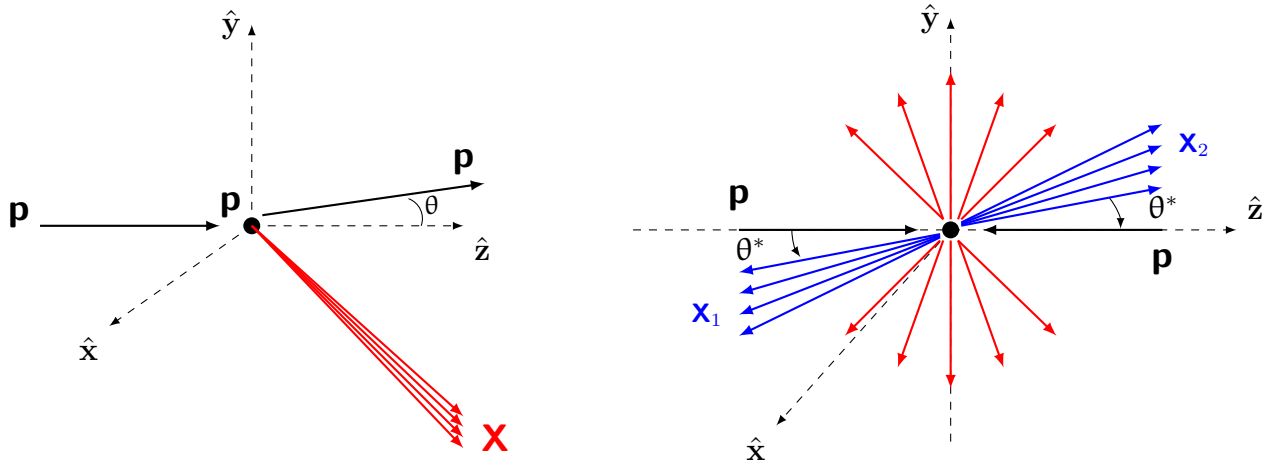

(a) **LAB** (b) **CM**

Figure 35: (a) An incident proton (**p**) collides with a stationary proton proton (**p**) in the LAB frame. (b) Collision of a proton (**p**) with another proton (**p**) in the CM frame. At the point of interaction occurs the multiple production of particles that come out in all directions, a special case is the jet production (the jets are $\mathbf{X}_1$ e $\mathbf{X}_2$).

A.1 Rapidity

$$y \equiv \frac{1}{2}\ln\left(\frac{\mathrm{E}+\mathrm{p_z}}{\mathrm{E}-\mathrm{p_z}}\right) \tag{10}$$

Rapidity differences are boost invariant.

$$\beta = \frac{\mathrm{p_z}}{\mathrm{E}}$$

in the $z-$direction

$$y \equiv \frac{1}{2}\ln\left(\frac{1+\beta}{1-\beta}\right)$$

A serie expansion for ln:

$$\ln\left(\frac{1+x}{1-x}\right) = 2x + \frac{2}{5}x^3 + \frac{2}{7}x^5 + ..., \quad -1 < x < 1 \tag{12}$$

using this expansion in the rapidity, we have

$$y = \frac{1}{2}\left(2\beta + \frac{2}{5}\beta^3 + \frac{2}{7}\beta^5 + ...\right) \tag{13}$$

In the limit $\beta \to 0$ (non-relativistic case)

$$y \simeq \beta + \mathrm{O}(\beta^3) \tag{14}$$

- Thus, in the non-relativistic case, the rapidity of a particle is equal approximately to the longitudinal velocity of the particle.
- Useful to treat the rapidity variable as a relativistically-invariant measure of longitudinal "velocity" of a particle [53].

To characterize the rapidity of a particle, it is necessary to measure the energy and momentum of the particle. In many experiments, it is only possible to measure the of the detected particle relative to the beam axis. In that case, it is convenient to utilize this information by using the pseudo-rapidity variable η to characterize the detected particle.

$$\eta = -\ln\left[\tan\left(\frac{\theta}{2}\right)\right] \tag{15}$$

where θ is the angle between the particle momentum $\vec{p}$ and the beam axis. it is easy to see that the pseudo-rapidity variable coincides when the momentum is large, that is, when $|\vec{p}| = E$ (limit m $\rightarrow 0$).

B High-Energy-Physics Event Generation with PYTHIA 8.2

Event generators generate simulated high-energy physics events. Despite the simple structure of the tree-level perturbative quantum field theory description of the collision and decay processes in an event, the observed high-energy process usually contains significant amount of modifications, like photon and gluon bremsstrahlung or loop diagram corrections, that usually are too complex to be easily evaluated in real calculations directly on the diagrammatic level. Any realistic test of the underlying physical process in a particle accelerator experiment, therefore, requires an adequate inclusion of these complex behaviors surrounding the actual process. Based on the fact that in most processes, a factorization of the full process into individual problems is possible (which means a negligible effect from interference), these individual processes are calculated separately, and the probabilistic branching between them are performed using Monte Carlo methods.

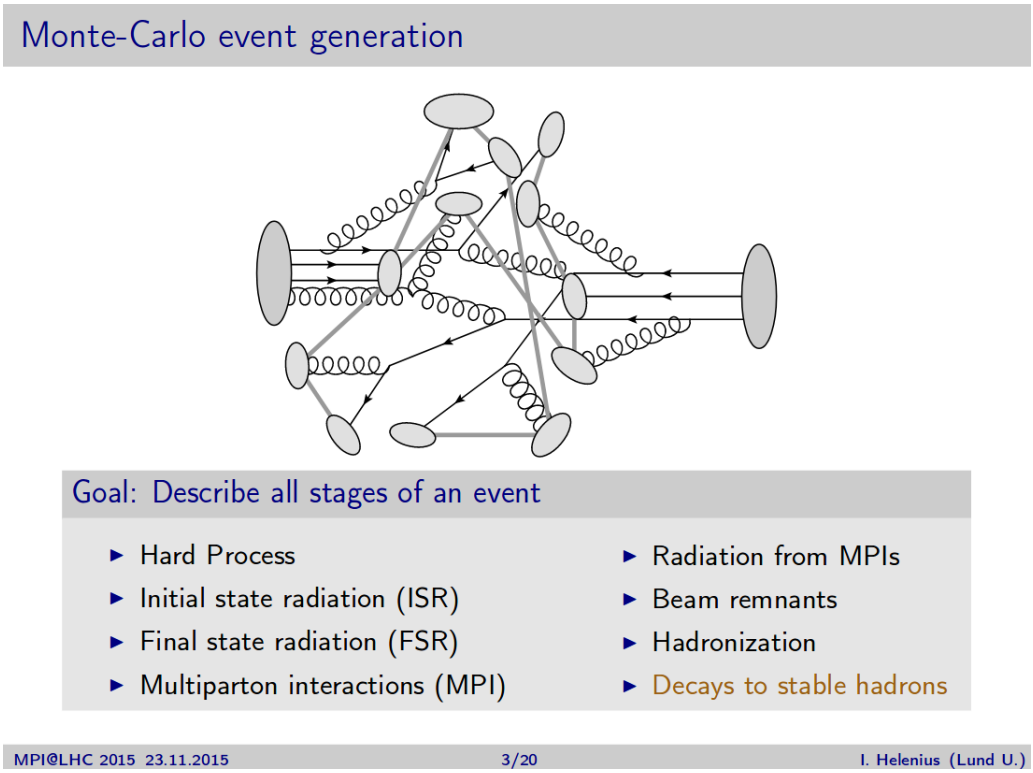

Figure 36: Description of the stage of an event generation.

- Theoretical tools that simulate events at colliders.
- Extensively used to simulate signal and background processes, to help us understand our data and enable us to make measurements.
- High p_T interactions are calculated using perturbation theory.
- Soft-QCD processes use phenomenological models with theoretical motivation that must be validated against data.

- These models contain parameters that must be tuned to the data.
- It is therefore necessary to make measurements of softQCD processes.

B.1 Hadronisation and Soft Hadron-Hadron Physics

- soft QCD that are relevant for hadron-hadron collisions, such as hadronisation, minimum-bias and soft-inclusive physics, and the so-called underlying event.
- In the event generators, hadronisation denotes the process by which a set of coloured partons (after showering) is transformed into a set of colour-singlet primary hadrons, which may then subsequently decay further.
- This non-perturbative transition takes place at the hadronisation scale $Q_{had} \sim 1$ GeV, which by construction is identical to the infrared cutoff of the parton shower. In the absence of a first-principles solution to the relevant dynamics, event generators use QCD-inspired phenomenological models to describe this transition.
- colour-singlet (i.e., confined) hadronic states. MC models do this in three steps:
  - Map the partonic system onto a continuum of high-mass hadronic states (called "strings" or "clusters").
  - Iteratively map strings/clusters onto discrete set of primary hadrons (via string breaks/-cluster splittings/cluster decays).
  - Sequential decays into secondaries ($\rho \to \pi\pi$, $\Lambda \to n\pi$, $\pi^0 \to \gamma\gamma$, ...).
- The physics governing this mapping is non-perturbative.

B.2 Minimum Bias

- Minimum bias adj. experimental term, to select events with the minimum possible requirements that ensure an inelastic collision occurred.
- Minimum Bias includes a diverse mixture of both soft and hard processes, though the fraction that is made up of hard high-p_T processes is only a small tail compared to the total minimum-bias cross section.
- In theoretical contexts, the term "minimum-bias" is often used with a slightly different meaning; to denote specific (classes of) inclusive soft-QCD subprocesses in a given model.

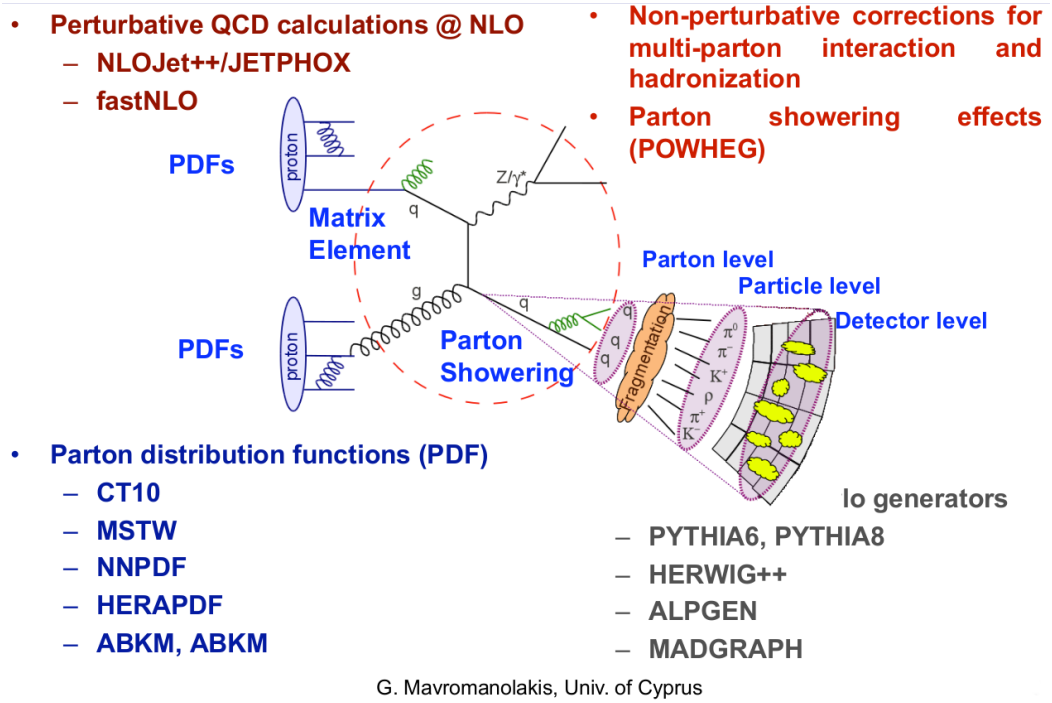

Figure 37

B.3 Underlying Event and Multiple Parton Interactions

- The physics of multiple parton interactions (MPI) as a theoretical basis for understanding both inelastic, non-diffractive processes (minimum-bias), as well as the so-called underlying event (a.k.a. the jet pedestal effect).
- hadrons are composite, multi-parton interactions (several dis- tinct parton-parton interactions in one and the same hadron-hadron collision) will always be there — but how many, and how much additional energy and tracks do they deposit in a given measurement region? The first detailed Monte Carlo model for perturbative MPI was proposed by Sjöstrand in [35, 54].

C SoftQCD

C.1 Non-Diffractive (ND)

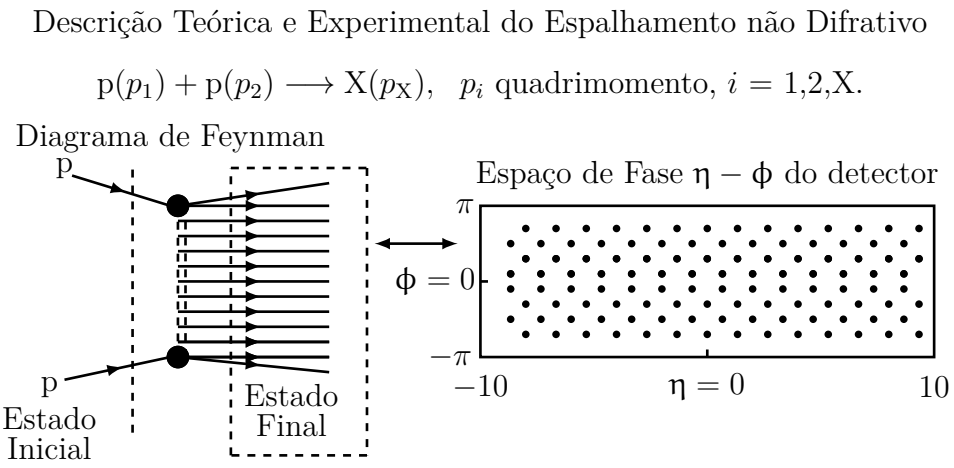

Figure 38: O diagrama de Feynman representa o processo de interação entre dois prótons, onde um Rapidity Gap (RG) é preenchida por partículas criadas no processo de hadronização.

C.2 Elastic Diffractive

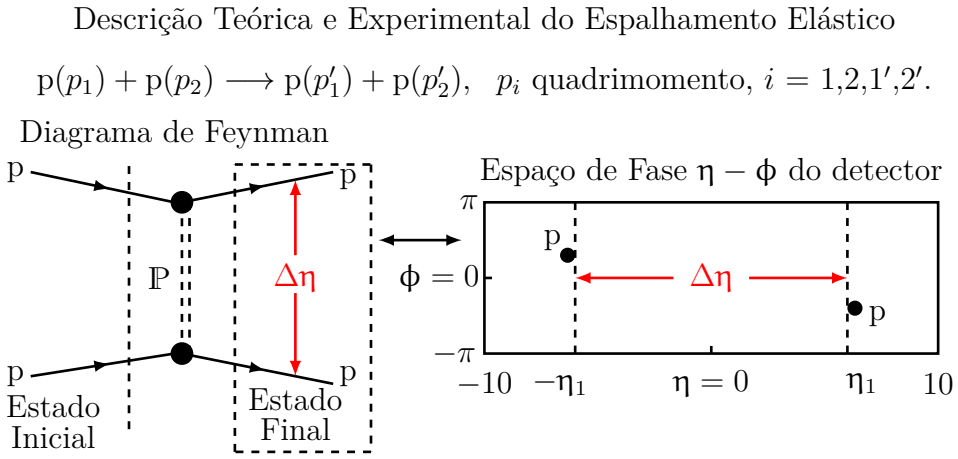

Figure 39: Diagrama de Feynman da interação entre os dois prótons e a distribuição dos prótons esperada para um espalhamento elástico. Com uma lacuna em pseudo-rapidez ($\Delta\eta$) no estado final.

C.3 Single Diffractive (SD)

Descrição Teórica e Experimental da Difração Simples (1º Caso)

$\mathrm{p}(p_1) + \Delta\eta + \mathrm{p}(p_2) \longrightarrow \mathrm{p}(p_3) + \mathrm{X}(p_\mathrm{X})$, p_i quadrimomento, i = 1,2,3,X.

Diagrama de Feynman

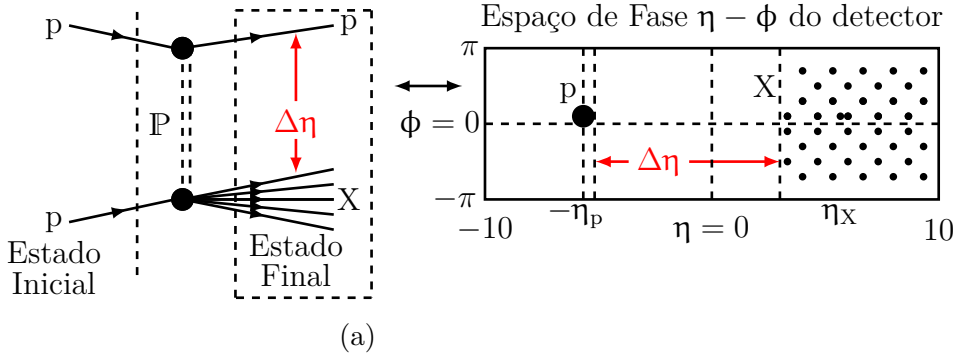

(a)

Descrição Teórica e Experimental da Difração Simples (2º caso)

$\mathrm{p}(p_1) + \Delta\eta + \mathrm{p}(p_2) \longrightarrow \mathrm{X}(p_\mathrm{X}) + \mathrm{p}(p_4)$, p_i quadrimomento, i = 1,2,X,4.

Diagrama de Feynman

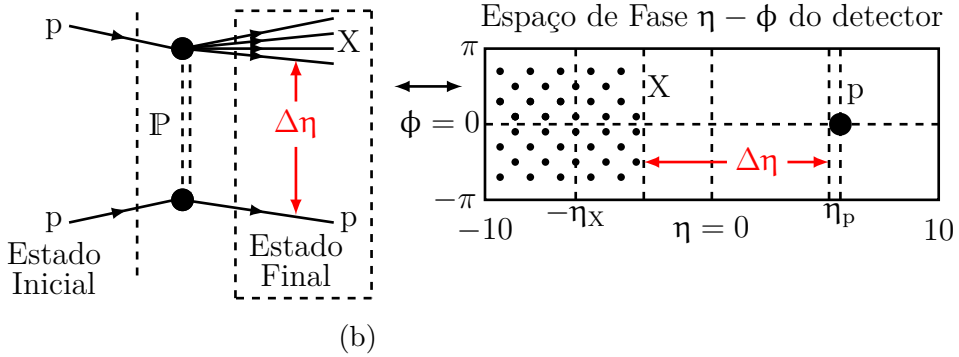

(b)

Figure 40: (a) O diagrama de Feynman representa a interação entre os prótons, através da troca do pomeron $\mathbb{P}$ e o que é esperado ser observado no espaço de fase $(\eta - \phi)$ do detector. Na região positiva em pseudorapidez o sistema difrativo **X** separado por um $\Delta\eta$ do próton na região negativa em pseudorapidez. (b) O diagrama de Feynman representa a interação entre os prótons, através da troca do pomeron $\mathbb{P}$ e o que é esperado ser observado pelo detector. Na região negativa em pseudorapidez o sistema difrativo **X** separado por um $\Delta\eta$ do sistema de prótons e na região positiva em pseudorapidez.

C.4 Double Diffractive (DD)

Descrição Teórica e Experimental da Difração Dupla

$$\mathrm{p}(p_1) + \Delta\eta + \mathrm{p}(p_2) \longrightarrow \mathrm{X}_1(p_{\mathrm{X}_1}) + \mathrm{X}_2(p_{\mathrm{X}_2}), \quad p_i \text{ quadrimomento, } i = 1{,}2{,}\mathrm{X}_1{,}\mathrm{X}_2.$$

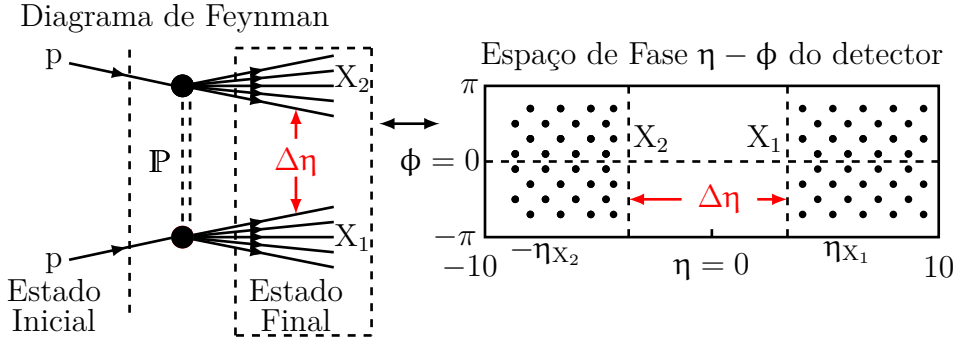

Figure 41: O diagrama de Feynman representa o processo de interação dos prótons através da troca do pomeron $\mathbb{P}$, com a dissociação dos prótons em dois sistemas de partículas X_1 e X_2 separados por um (RG), na região central em pseudorapidez observada no espaço de fase do detector.

D Dados de Raios Cósmicos Observados pela CBJ

Os dados disponíveis para análise são referentes aos eventos observados nas câmaras inferiores (Tabela 3). A partir desses dados foram construídas as seguintes distribuições: de partículas em função da pseudorapidez (η), de energia em função da pseudorapidez (η), de partículas em função do ângulo azimutal (ϕ) e de momento transversal (p_T). As distribuições são fundamentais na busca por uma compreensão dos processos de interação hadrônica que ocorrem na câmara superior.

Table 3: Dados das Câmaras Inferiores

Nº	Evento	Nº Chuveiros	$\sum E_\gamma$ [TeV]	Nº	Evento	N° Chuveiros	$\sum E_\gamma$ [TeV]
1	1517	9	20.97	34	17961	28	33.66
2	1528	16	30.34	35	17962	19	20.10
3	1543	18	24.74	36	171022	26	31.88
4	1547	9	92.55	37	171024	21	22.14
5	1567	25	21.76	38	17104	12	23.23
6	156725	19	24.68	39	17105	5	32.32
7	1576	15	19.67	40	17115	14	18.51
8	1577	14	27.94	41	17122	10	22.35
9	1584	17	18.70	42	17124	23	44.38
10	1597	24	62.53	43	17130	18	38.94
11	15102	22	34.06	44	17132	5	25.10
12	15105	22	35.02	45	171351	29	38.66
13	15115	29	76.62	46	171354	21	23.69
14	15150	8	19.38	47	17136	37	110.48
15	15156	4	24.85	48	171382	14	21.08
16	15159	9	22.97	49	171388	25	19.82
17	151614	6	16.91	50	17140	27	30.37
18	1680	25	36.86	51	17148	19	19.32
19	1685	4	20.85	52	17150	12	95.15
20	1686	9	118.75	53	17159	13	21.31
21	1691	24	31.49	54	17164	44	123.20
22	1696	15	24.02	55	1821	5	65.93
23	16101	16	52.75	56	1824	17	28.34
24	16105	26	26.23	57	1828	4	29.30
25	17192	23	95.27	58	1830	22	65.86
26	1769	7	32.25	59	1832	22	54.14
27	17791	4	31.10	60	1847	13	24.20
28	17792	7	34.44	61	1849	26	42.74
29	17841	8	23.54	62	1869	22	42.64
30	17842	11	22.45	63	187330	20	26.85
31	1786	28	40.83	64	187650	13	21.91
32	1789	7	25.81	65	1892	18	18.49
33	1790	27	41.91	66	1893	14	27.16

Nº	Evento	N° Chuveiros	$\sum E_\gamma$ [TeV]
67	18110	27	37.20
68	18139	19	20.17
69	18145	8	37.93
70	18149	8	69.65
71	19100	7	25.90
72	19105	12	21.40
73	19107	8	21.29
74	19108	11	24.14
75	19115	12	57.45
76	191214	8	21.30
77	191215	8	20.19
78	19127	19	21.51
80	191361	15	52.46
81	191362	16	81.45
82	19138	9	29.00
	TOTAL	1334	

- $<$ 20 TeV $\rightarrow$ 8 Eventos.
- 20 - 30 TeV $\rightarrow$ 36 Eventos.
- 30 - 40 TeV $\rightarrow$ 16 Eventos.
- 40 - 50 TeV $\rightarrow$ 5 Eventos.
- 50 - 60 TeV $\rightarrow$ 4 Eventos.
- 60 - 70 TeV $\rightarrow$ 4 Eventos.
- 70 - 80 TeV $\rightarrow$ 1 Evento.
- 80 - 90 TeV $\rightarrow$ 1 Evento.
- 90 - 100 TeV $\rightarrow$ 3 Eventos.
- 110 - 123 TeV $\rightarrow$ 4 Eventos.